Accuracy of Regularized Differential Operators for Discontinuity Localization in 1-D and 2-D Intensity Functions

Heiko Neumann[1], Karsten Ottenberg[2], H. Siegfried Stiehl[1]

FBI-HH-M-186/90

October 1990

[1]Universität Hamburg, Fachbereich Informatik
Bodenstedtstr. 16, D-2000 Hamburg 50 (FRG)

[2]Philips Forschungslaboratorium Hamburg
Vogt-Kölln-Str. 30, D-2000 Hamburg 54 (FRG)

Abstract

For the purpose of theoretically assessing the performance of differential operators for computational discontinuity localization, we investigate here the localization capability of regularized first and second order differential operators given a variety of continuous image structure. For the 1-D case, we are concerned with mathematical notations for common models of one-dimensional intensity functions for which we analyze the performance of different operators with respect to their intrinsic localization error. For the 2-D case, we propose the scalable cylinder model of curved intensity variations as a generalization of both the 1-D step and the ramp edge model. In particular, we analyze the intrinsic localization error of the Laplacian operator (with the Laplacian of Gaussian as the regularized filter kernel), and the first as well as the second order directional derivative (with the corresponding derivative of the Gaussian as the regularized filter kernel) for different parametrizations of the cylinder model (e.g. radius and scale of discontinuity). Novel results from analytical and numerical solutions will be presented and discussed for both the 1-D and the 2-D case.

published in:

Haralick, R.M.; Förstner, W. (Eds.)

Proceedings of the First International
IEEE Workshop on Robust Computer Vision
Seattle, WA, USA, 1-3 October 1990

(to be published by Academic Press, 1991)

Zusammenfassung

Mit dem Ziel einer Beurteilung der Performanz von Differentialoperatoren zur Lokalisation von Diskontinuitäten in ein- und zweidimensionalen Signalen, wird in dieser Arbeit die Lokalisationsgenauigkeit von regularisierten Differentialoperatoren 1. und 2. Ordnung für eine Reihe von prototypischen kontinuierlichen (Bild-) Strukturen theoretisch untersucht. Für den eindimensionalen Fall betrachten wir für allgemeine, in der internationalen Literatur häufig diskutierte Modelle eindimensionaler Intensitätsfunktionen, für die wir die Performanz verschiedener Operatoren im Hinblick auf ihre intrinsischen Lokalisationsungenauigkeiten analysieren. Für den zweidimensionalen Fall schlagen wir das Modell eines skalierbaren Zylinders - als Verallgemeinerung eines 1-D Sprungkanten- und Rampenmodells - vor, auf dessen Grundlage lokale Intensitätsvariationen unterschiedlicher Flächengeometrien angenähert werden können. Im einzelnen untersuchen wir den intrinsischen Lokalisationsfehler des Laplace-Operators (mit dem Laplace der Gaußfunktion als regularisiertem Filteroperator) und sowohl der ersten als auch zweiten Richtungsableitung der Bildfunktion (mit der jeweiligen Ableitung 1. bzw. 2. Ordnung der Gaußfunktion als korrespondierende regularisierte Filteroperatoren) für verschiedene Parametrisierungen des Zylindermodells, z.B. Radius und Skalierung der Diskontinuität. Neue Ergebnisse analytischer und numerischer Lösungen werden gezeigt und für den ein- bzw. zweidimensionalen Fall diskutiert.

erschienen in:

Haralick, R.M.; Förstner, W. (Eds.)

Proceedings of the First International
IEEE Workshop on Robust Computer Vision
Seattle, WA, USA, 1-3 October 1990

(erscheint bei Academic Press, 1991)

Accuracy of Regularized Differential Operators for Discontinuity Localization in 1-D and 2-D Intensity Functions

Heiko Neumann†, Karsten Ottenberg‡, H.Siegfried Stiehl†

†Universität Hamburg, Fachbereich Informatik
Bodenstedtstr.16, D-2000 Hamburg 50, Europe

‡Philips Forschungslaboratorium Hamburg
Vogt-Kölln-Str.30, D-2000 Hamburg 54, Europe

Abstract. For the purpose of theoretically assessing the performance of differential operators for computational discontinuity localization, we investigate here the localization capability of regularized first and second order differential operators given a variety of continuous image structure. For the 1-D case, we are concerned with mathematical notations for common models of one-dimensional intensity functions for which we analyze the performance of different operators with respect to their intrinsic localization error. For the 2-D case, we propose the scalable cylinder model of curved intensity variations as a generalization of both the 1-D step and the ramp edge model. In particular, we analyze the intrinsic localization error of the Laplacian operator (with the Laplacian of Gaussian as the regularized filter kernel), and the first as well as the second order directional derivative (with the corresponding derivative of the Gaussian as the regularized filter kernel) for different parametrizations of the cylinder model (e.g. radius and scale of discontinuity). Novel results from analytical and numerical solutions will be presented and discussed for both the 1-D and the 2-D case.

Contents

1. Introduction and Motivation

Considering computational (or machine) vision processes as a quantitative analysis and mensuration t
[22], e.g. a calibrated instrument for remote sensing or medical domain applications, provokes awkw
questions related to common engineering requirements such as accuracy, reliability, reproducibility, corr
ness, and robustness. Following the metaphor of a calibrated delicate instrument, a potential user i
particular task- and domain-specific situation has to strive for being assured of a guarantee for an abso
minimum or maximum error maybe even in terms of a fidelity certificate. In domains where accuracy
critical issue, the user of a machine vision based instrument - given a task specification - thus has to m
the best choice between a variety of instruments on the basis of facts derived from either the theoretic
or experimentally proven scientific frontier [21].

In the context of computational vision, and particularly for discontinuity localization, the main iss
related to such an envisaged fidelity measure are [42]:

- The selection of an approach for evaluation and comparision of the performance of operators,
- the objective determination of the superiority of a particular operator with respect to the actual ta
  and
- the assessment of the generality of the operator with respect to the prevailing image structure.

Although no general theory for performance and robustness evaluation of operators for computatio
discontinuity localization does exist so far, a plethora of scientific papers addressed this issue in the pa
The attempts may be broadly categorized as follows:

a) Starting either from mathematical models of receptive fields known from neurobiology or from pr
   determined performance criteria, continuous operators are defined in an analytical form, and sub
   quently the performance is theoretically validated or theoretically evaluated by a comparative a
   competitive assessment of the performance (via an analytic solution in the ideal case).

b) Discrete operators are designed, e.g. by appropriately sampling continuous ones, followed by a s
   sequent validation assessment in either qualitative terms via pure visual inspection of the resu
   verbally explicated empiry, or quantitative terms via tables of fidelity measures.

In any case, the validation or assessment requires data, which are either given by continuous models
the expected image structure or discrete images believed to possess typicality. While continuous mod
so far have been defined only for the classical step edge and, only recently, for the ramp edge, the va
of definition of discrete test image data is still under dispute ([42]; see also [17] for early attempts). W
respect to the above mentioned dichotomy, this categorization may be also considered as a valid strate
in the sense of continuous case at first and discrete case at second. However, this non-trivial approa
requires both, a mathematically tractable definition of the theoretical problem and, in a painstaking w
the consideration of sampling, tesselation, quantization, and noise side effects. In addition, the realizatio
a carefully defined and controllable experimental testbed as well as a thorough definition of a test strate
would be of paramount importance (if not a methodological prerequisite) to assure valid scientific resu
(see [35] for a proposal).

We oppose the purely experimental validation and assessment of operators, but argue in favour of a th
retical analysis of the continuous case to a maximum extent prior to discrete case experiments (provi

that this is possible for a particular problem). Why? Above all, only such an endeavour guarantees to prove the intrinsic theoretical error limits in the sense of an lower- or upper-bound error from which precise local or global measures for operator performance can be derived which are clearly beyond primae facie evidence from visual inspection (the worst but still practized case) of the results of operators for discontinuity localization. Following this line of strengthening the theoretical basis of computational vision, we will in a paradigmatic way present novel analytical models of a variety of 1-D and 2-D continuous image structure (including scale of discontinuities by Gaussian blurring) along with analytical and numerical solutions to the problem of assessing the localization performance of regularized differential operators for discontinuity localization in the continuous case.

After having motivated our research, we will briefly introduce the basic ideas and concepts explicated in detail in the remainder of this paper. As argued above, accurate, reliable, and stable numerical solutions for the ill-posed problem of discontinuity localization play an important role in early computational vision. Paradigmatic work on regularization to achieve numerical stability was reported in e.g. [45] and [3]. It has been shown, for instance, that the Gaussian filter is a valid approximation of the optimal regularization filter, derived theoretically from an underlying optimization problem. Beside the Gaussian filter generating the scale of the discontinuities within our intensity models, we also have to consider a second Gaussian filter for the regularization of the ill-posed differential operators in our analysis. We distinguish between the two different Gaussian kernels by referring to their standard deviations as σ_{mod} and σ_{reg} respectively.

While the numerical stability of this type of regularized operators has been investigated in detail (see e.g. [45] and [3]), a theoretical analysis of the *accuracy* of discontinuity localization schemes, leading to quantitative results, has not been yet addressed in full detail.

For the purpose of arriving at mathematical foundations for discontinuity localization schemes and allowing for a precise validation of the performance of different operators, models of discontinuities have been recognized to be essential. Discontinuity models such as step edges ([12], [34], [20]) and arbitrarily scaled ramps ([46], [27], [4]) have been proposed in the past. However, a thorough and complete competitive and comparative assessment of the ability of operators to both reliably detect and accurately localize discontinuities has not been achieved in the past.

Although the detailed discussion of the previous work on the problem of 1-D and 2-D discontinuity localization will be done within the discussions of our own results for the 1-D and 2-D case respectively, we want to summarize some general aspects of this work here.

It has been shown only for specific cases that even for ideal, viz. continuous and noiseless, intensity functions the operator response cannot be predicted per se due to either the degrees of freedom of local intensity variations ([33], [37]), or the intrinsic deficiencies of operators. With respect to the latter, Berzins [7] for instance reported on zero crossing displacements around the location of an ideal V-junction in 2-D intensity functions, while Clark [15] in his analysis of staircase shaped intensity functions even observed phantom zero crossings. In addition to these general problems, the numerical realization of operators, as they have been mathematically defined for the continuous case, degrades their theoretically predicted localization capability. The discrete nature of sampled intensity functions with, e.g. additive Gaussian, noise additionally prevents from predictable results once operators usually defined for the 1-D continuum are applied to discrete images. As a consequence, Lunscher and Beddoes [29] carefully analyzed filter parameter design which is an indispensable prerequisite to achieve accurate and reliable results in the presence of noise.

Apart from the localization problem, the scale problem, e.g. step edges *and* arbitrary ramp edges at prior unknown image locations, inheres also in discontinuity localization. Only recently, a small number of

papers addressed the severe problem of scale in discontinuity localization and proposed numerical multi-scale integration schemes to appropriately combine operator responses from multiple scales ([46], [27], [4]).

Finally, it can be safely stated that another major drawback in 2-D computational discontinuity localization is the common premise of 1-D discontinuity models, e.g. particularly one-dimensional image intensity functions which are assumed to be

a) coplanar with the cutting plane along the local gradient direction and

b) to have zero principal curvatures at least in its inflection point.

As a consequence of this basic assumption of a linear replicative variation of the 1-D discontinuity model along the tangent direction, 2-D discontinuity localization operators expectedly exhibit only sub-optimal performance in the presence of a higher complexity of intensity surfaces with respect to differential geometry. For a detailed discussion see section 2.3 on the results of the 1-D discontinuity models and section 3.3 on the results of the 2-D cases.

In the following chapters of this paper we will thus particularly investigate the localization capability of different operators with respect to a variety of local intensity functions in 1-D and in 2-D from a theoretical point of view. For the 1-D case, regularized first and second order derivatives as applied to step edges, ramps, roofs and bars (also undergoing Gaussian blurring) will be analyzed in depth. For the 2-D case, we will extend the 1-D step and ramp edge model to a cylinder model with control of local differential geometry via independent parametrization of radius, contrast, and discontinuity scale.

To briefly recapitulate, discontinuity localization schemes have been usually derived from the 1-D continuum, whereas for the case of 2-D intensity functions only the assumption of a linear replication of 1-D intensity variation models in tangent direction assures optimal localization capabilities. For the 2-D case, it has been argued that precise discontinuity localization hence has to be carried out for one-dimensional discontinuities only (generated by cutting planes in 2-D intensity surfaces that contain the intensity axis ($< 0, 0, f(x, y) >$), thus treating the problem as for the 1-D case but for different orientations (see [2]). However, this approach necessarily requires a number of differently oriented (1-D) convolutions, interpolation on the 2-D regular grid and a subsequent interpolation between the different operator outputs for the sampled orientation space. Motivated by the research on discontinuity localization based upon the Laplacian of Gaussian at first reported in [30], the performance of Laplacian of Gaussian based discontinuity localization has been compared to the non-linear second order directional derivative in the gradient direction (which yields the true edge location, see e.g. [45], [20]). Based on Canny's optimization approach [12] in order to find a more robust operator for localization of 1-D step edges with respect to stability in case of noise, a great amount of approaches favoured directional operators based on the first order derivative (e.g. [27], [4]). Therefore, we concentrated in our 2-D analysis on the localization capability of the Laplacian of Gaussian and the first order directional derivative operator with respect to curved and scaled intensity functions related to the cylinder model.

2. Discontinuity Localization in 1-D Intensity Functions

2.1 Models of 1-D Intensity Functions

In this chapter we will investigate the intrinsic localization accuracy of regularized first and second order differential operators for four different 1-D discontinuity models as proposed in [33] and [37], respectively. In particular, the examined intensity functions in 1-D are the ideal step, the ramp, the bar (or pulse) and the roof. The *step* edge is the most frequently used model in the development and evaluation of discontinuity detection and localization schemes (see e.g. [7], [20], [12], [19]). This simplest type of intensity function models a sudden change in the brightness function which in turn represents either a single physical cause or a combination of such causes ([31]). A *ramp* edge is a coarse approximation of an extended, i.e. smooth, transition between two neighboring intensity niveaus. These two idealized intensity functions approximate local contrast changes over a spatial range of different locations. Combinations of these contrast changes have been considered as specific image structure primitives, since they may be covered by the significant spatial support of a particular operator of finite extent therefore contributing to operator response. The most popular representatives of such models are the bar and the roof, respectively. The *bar* (or *pulse*) represents a one-dimensional cut through a light intensity line stroke on a dark background. The standard bar primitive can thus be synthesized by two steps of equal contrast magnitude but inverse polarity. By reversing the order of combination of the two steps with respect to a particular traversing direction, a cut through a dark line on bright background is modelled. This type of intensity variation is sometimes called a *slit* (see [37]). The *roof* is simply generated by two ramps with an opposite sign of slope. This special type of intensity variation has been observed to occur in images of concave geometry discontinuities of polyhedral surfaces ([23]). Figure 1 (a)-(d) provides a sketch of these functions also indicating the inherent free parameters for definition of the functions.

The simple bar function introduced above was defined as a combination of two separated steps of equal magnitude but inverse polarity. This definition can be relaxed by introducing a relative contrast ratio a (see also [41]). Therefore, we can construct bar shaped intensity functions with neighbouring regions of different intensity niveaus, which we subsequently refer to as *generalized bars*. By inverting the sign of the ratio a, the commonly known *staircase* model can be synthesized. In the case of two combined step changes of equal polarity (corresponding to $a = -1$) a two-step stair is generated. Figure 1 (e), (f) shows sketches of a generalized bar and a staircase, both for ratios a in the interval $[0, 1]$ and $[-1, 0]$, respectively.

2.2 Accuracy of Localization for the Standard 1-D Models

For the general 1-D case, discontinuity detection by finding local extrema in the first order derivative of the intensity function is identical to discontinuity detection by finding zero crossings of its second order derivative. We thus can restrict our analysis to solve for zero crossings of the second order derivatives for each of the different discontinuity models introduced above.

Let $\mathcal{H}$ denote the Heaviside function, defined by

$$\mathcal{H}(x) = \begin{cases} 0 & \text{if } x < 0 \\ 1 & \text{if } x \geq 0 \end{cases}$$

(see [39]). A **step edge** discontinuity in an intensity function with positive flank located at position $x = Z$ and local contrast c, can then be denoted by

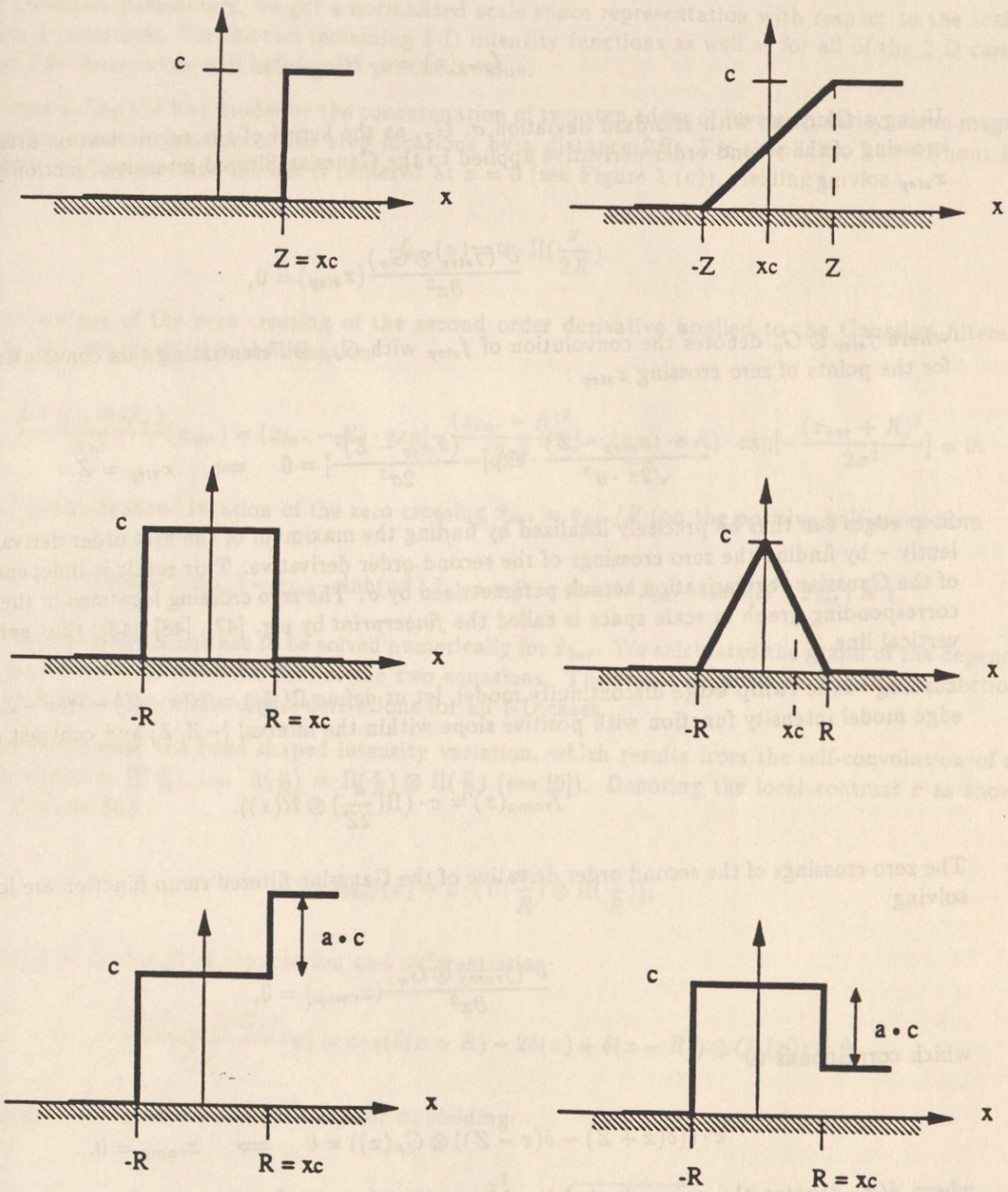

Figure 1: Different types of 1-D intensity functions (without Gaussian blurring) analyzed in this section; (a) step, (b) ramp, (c) bar (pulse), (d) roof, (e) generalized bar, and (f) staircase ((e) and (f) with contrast ratios $0 < a < 1$) (for intensity variations scaled by Gaussian blurring, see Section 2.2); x_c denotes the true location of the discontinuity used as the reference in our derivations.

$$f_{step}(x) = c \cdot \mathcal{H}(x - Z).$$

Using a Gaussian with standard deviation σ, G_σ, as the kernel of the regularization filter ([45]), the zero crossing of the second order derivative applied to the Gaussian filtered intensity function f_{step} is located at x_{step} solving

$$\frac{\partial^2 (f_{step} \otimes G_\sigma)}{\partial x^2}(x_{step}) = 0,$$

where $f_{step} \otimes G_\sigma$ denotes the convolution of f_{step} with G_σ. Differentiating this convolution twice, we find for the points of zero crossing x_{step} :

$$\frac{-c \cdot (x_{step} - Z)}{\sqrt{2\pi} \cdot \sigma^3} \cdot \exp[-\frac{(x_{step} - Z)^2}{2\sigma^2}] = 0 \quad \Longrightarrow \quad x_{step} = Z. \tag{1}$$

Step edges can thus be precisely localized by finding the maximum of the first order derivative or – equivalently – by finding the zero crossings of the second order derivative. This result is independent of the scale of the Gaussian regularization kernel, parametrized by σ. The zero crossing locations in the scale space (the corresponding graph in scale space is called the *fingerprint* by e.g. [47], [48], [43]) thus generate a straight vertical line.

Turning to the **ramp edge** discontinuity model, let us define $\Pi(\frac{x}{2Z}) = \mathcal{H}(x + Z) - \mathcal{H}(x - Z)$. For the ramp edge model intensity function with positive slope within the interval $[-Z, Z]$ and contrast c we can denote

$$f_{ramp}(x) = c \cdot (\Pi(\frac{x}{2Z}) \otimes \mathcal{H}(x)).$$

The zero crossings of the second order deivative of the Gaussian filtered ramp function are located at x_{ramp}, solving

$$\frac{\partial^2 (f_{ramp} \otimes G_\sigma)}{\partial x^2}(x_{ramp}) = 0,$$

which corresponds to

$$c \cdot ((\delta(x + Z) - \delta(x - Z)) \otimes G_\sigma(x)) = 0 \quad \Longrightarrow \quad x_{ramp} = 0. \tag{2}$$

where $\delta(x)$ denotes the generalized delta function. We thus find that the localization of a ramp edge discontinuity by first and second order derivatives is precise as well. Therefore, its fingerprint in scale space is identical to that of the ideal step, namely a straight line.

Before we investigate the bar (pulse) and the roof, let us now introduce two useful parameters.

- First, we rescale x by normalizing it with respect to the radius R (half the width) of the corresponding structure (e.g. bar and roof), $\hat{x} = x/R$.

- Second, we define the ratio $\alpha = R/\sigma$, where R is half the width of the structure and σ is the standard deviation of the Gaussian regularization filter.

Using these two parameters, we get a normalized scale space representation with respect to the scaling of individual primitives. For the two remaining 1-D intensity functions as well as for all of the 2-D cases (see Section 3.2) these ratios will be of great practical value.

Let us now define the **bar** model by the concatenation of two step edges of inverse polarity, same magnitude of contrast c and separation of the step locations by a distance $2R$. For simplicity, but without loss of generality, we assume that the bar is centered at $x = 0$ (see Figure 1 (c)), yielding

$$f_{bar}(x) = c \cdot \Pi(\frac{x}{2R}).$$

For the location of the zero crossing of the second order derivative applied to the Gaussian filtered bar function f_{bar}, we must solve the equation

$$\frac{\partial^2(f_{bar} \otimes G_\sigma)}{\partial x^2}(x_{bar}) = (x_{bar} - R) \cdot \exp[-\frac{(x_{bar} - R)^2}{2\sigma^2}] - (x_{bar} + R) \cdot \exp[-\frac{(x_{bar} + R)^2}{2\sigma^2}] = 0.$$

We find the normalized location of the zero crossing $\hat{x}_{bar} = x_{bar}/R$ (on the positive half axis) from

$$\cosh(\alpha^2 \cdot \hat{x}_{bar}) - \hat{x}_{bar} \cdot \sinh(\alpha^2 \cdot \hat{x}_{bar}) = 0 \iff \hat{x}_{bar} \cdot \tanh(\alpha^2 \cdot \hat{x}_{bar}) = 1. \tag{3}$$

One of these two equations has to be solved numerically for $\hat{x}_{bar}$. We calculated the graph of the dependence of $\hat{x}_{bar}$ on the ratio α from the first of the two equations. The result is shown in Figure 2 in Section 2.3 where we discuss the results of the derivations for all 1-D cases.

Next, we investigate the **roof** shaped intensity variation, which results from the self-convolution of a bar intensity function $\Pi(\frac{x}{R})$, i.e. $\Lambda(\frac{x}{R}) = \Pi(\frac{x}{R}) \otimes \Pi(\frac{x}{R})$ (see [9]). Denoting the local contrast c as shown in Figure 1 (d) we find

$$f_{roof}(x) = c \cdot (\Pi(\frac{x}{R}) \otimes \Pi(\frac{x}{R})),$$

which leads to the result of convolution and differentiation:

$$\frac{\partial^2(f_{roof} \otimes G_\sigma)}{\partial x^2}(x) = c \cdot ((\delta(x + R) - 2\delta(x) + \delta(x - R)) \otimes G_\sigma(x)) = 0.$$

This equation can be solved analytically for x, yielding

$$\hat{x}_{roof} = \frac{1}{\alpha^2} \cdot \ln[\exp(\frac{\alpha^2}{2}) + \sqrt{\exp(\alpha^2) - 1}] \tag{4}$$

for the normalized zero crossing location $\hat{x}_{roof} = x_{roof}/R$. A graph of the dependence of $\hat{x}_{roof}$ on the ratio α is given in Figure 3 also in Section 2.3.

As we have argued above, the **generalized bar** function can be simply defined by introducing the contrast ratio a into the equation for the simple bar, which then yields the following expression for the generalized bar intensity function:

$$f_{gbar}(x) = c \cdot (\mathcal{H}(x - R) - a \cdot \mathcal{H}(x + R)).$$

For the second order derivative of this function convolved with the Gaussian, we find

$$\frac{\partial^2 (f_{gbar} \otimes G_\sigma)}{\partial x^2}(x) = \frac{c}{\sqrt{2\pi} \cdot \sigma^3} \cdot (x - R) \cdot \exp[-\frac{(x - R)^2}{2\sigma^2}] - (x + R) \cdot \exp[-\frac{(x + R)^2}{2\sigma^2}],$$

while for the zero crossing $\hat{x}_{gbar}$ we arrive at the equation

$$a \cdot \exp(\alpha^2 \hat{x}_{gbar}) + \exp(-\alpha^2 \hat{x}_{gbar}) - \hat{x} \cdot [a \cdot \exp(\alpha^2 \hat{x}_{gbar}) - \exp(-\alpha^2 \hat{x}_{gbar})] = 0.$$

Using the identities $e^{ax} = \cosh(ax) + \sinh(ax)$ and $e^{-ax} = \cosh(ax) - \sinh(ax)$ we finally yield

$$(a+1) \cdot \cosh(\alpha^2 \cdot \hat{x}_{gbar}) + (a-1) \cdot \sinh(\alpha^2 \cdot \hat{x}_{gbar}) - \hat{x}_{gbar} \cdot [(a-1) \cdot \cosh(\alpha^2 \cdot \hat{x}_{gbar}) + (a+1) \cdot \sinh(\alpha^2 \cdot \hat{x}_{gbar})] = 0 \quad (5)$$

For $a = 1$ this equation reduces to the one we have derived above for the case of a simple bar function (eqn. (4)). Again, we have to apply a numerical scheme to find the roots of this equation. Figure 4 in Section 2.3 shows the graphs of the zero crossing locations for different contrast ratios $0 < a \leq 1$ (Figure 4 (a)) and $a > 1$ (Figure 4 (b)).

As described in Section 2.1, the **staircase** model of local intensity functions is derived from the one for the generalized bar by simply changing the sign of the ratio of the individual contrast magnitudes of the two steps. It has to be noted here that for the staircase certain problems arise if the discontinuity detection scheme is based on finding zero crossings in the second order derivative of the Gaussian filtered staircase. Whereas maxima of the first order derivative occur at the positions of the two individual flanks only, the zero crossing locations of the second order derivative correspond to inflection points in the filtered function, i.e. local extrema (maxima *and* minima) of the first order derivative. Therefore, in addition to the zero crossings at the locations of local maxima of the first order derivative, an additional discontinuity point candidate occurs between the two step locations. This zero crossing was first investigated by Clark [14] (see also [15]) and characterized as a *phantom edge*. Several methods have been proposed for its classification from the zero crossings in 1-D and 2-D intensity functions. This problem is beyond the scope of our paper, but the reader is forwarded to the literature cited above (see also [25]).

For the numerical solution for the zero crossing locations of the staircase intensity function, eqn.(5) is parametrized with contrast ratios $a < 0$. For convenience, eqn.(5) has been rewritten such that positive values of a enter into the equation, yielding

$$(1-a) \cdot \cosh(\alpha^2 \cdot \hat{x}_{gbar}) - (1+a) \cdot \sinh(\alpha^2 \cdot \hat{x}_{gbar}) + \hat{x}_{gbar} \cdot [(1+a) \cdot \cosh(\alpha^2 \cdot \hat{x}_{gbar}) - (1-a) \cdot \sinh(\alpha^2 \cdot \hat{x}_{gbar})] = 0 \quad (6)$$

The graphical representations of the results for zero crossing locations are shown in Figure 5. The illustrations are separated for results of $0 < |a| < 1$ (Fig. 5 (a)) and $|a| > 1$ (Fig. 5 (b)) and presented as well as discussed in Section 2.3.

This concludes the derivation of the equations of zero crossing locations of the second order derivative of Gaussian filtered 1-D intensity functions depicted in Figure 1 (a)-(f). All models investigated so far have not taken into account the possible scaling of the structure by prior blurring with Gaussian, in order to generate e.g. differently scaled discontinuities of error integral type or ridge like structures. How does such a scaling of the structure influence our results ? Let σ_{mod} be the standard deviation of the blurring Gaussian, and denote the standard deviation of the Gaussian used for regularization as σ_{reg} (corresponding to σ in the preceding formulas). The combined effect of the convolution of an intensity function with the two Gaussian kernels is equal to the convolution of this function with a single Gaussian kernel with standard deviation $\sigma_{eff} = \sqrt{\sigma_{reg}^2 + \sigma_{mod}^2}$. Therefore, all results derived for the step, ramp, simple bar, roof, generalized bar, and staircase model hold true. We only have to rescale the original α within all formulas to $\tilde{\alpha} = (\sigma_{reg}/\sqrt{\sigma_{reg}^2 + \sigma_{mod}^2}) \cdot \alpha$, while all the $\hat{x}'s$ remain unchanged.

2.3 Discussion of Results

In this chapter, we will discuss the results of the numerical solution to discontinuity localization based upon the normalized scale space representation, and we relate our results to those reported in the literature.

Let us first give a short review of the most relevant contributions from the literature. Within the numerous publications, most investigations and analyses of linear discontinuity localization operators were made on the basis of the ideal step edge model. Basically, the publications can be classified into two groups (corresponding to the dichotomy introduced in Chapter 1).

First, operators have been designed and optimized with respect to performance criteria, such as localization, uniqueness and noise insensitivity. Among these we believe the works of Canny (e.g. [12]) and L.Spacek ([44]) to be the most important. Canny in [10], [11] and [12] proposed an optimization approach to operator design in order to derive optimally suited operators for the detection and localization of discontinuities in different 1-D intensity functions. The criteria which served as the basis for his optimization procedure have been selected with respect to the uniqueness of operator response in case of disturbance of the signal, localization accuracy of the estimated point of discontinuity and noise insensitivity. Canny was able to derive optimally suited operators for step edges and bar intensity functions. The corresponding filter kernel derived for the step edge operator was similar to the first order derivative of a Gaussian.

Following Canny's work, Spacek [44] in a theoretical paper thoroughly investigated the design of a 1-D finite width step edge localization operator on the basis of the first order derivative. In particular he developed three analytical criteria for the design of an *optimal* operator which are expressed via quantitative performance measures. Given a composite functional which combines analytical performance measures for signal strength (e.g. signal-to-noise ratio), localization accuracy and noise suppression, Spacek derived an analytical solution for this optimum operator by maximization of a quadratic functional using standard variational calculus. The same principles were applied to the design of an operator which optimizes the noise suppression measure only. Spacek further provided a detailed comparison of his optimal (cubic spline) operator with the Canny operator based on the quantitative performance measures mentioned above.

In correspondence to the first class of the dichotomy introduced in Chapter 1, we review former work on the analysis of operators which have been defined on the basis of some prior given filter kernel (such as the Gaussian). As it can be immediately seen from our motivation, our own work reported in this article belongs to this type of approach.

Shah et al. [43] qualitatively investigated the localization capability of the Laplacian of Gaussian operator for isolated 1-D ideal step, ramp, bar (pulse), and staircase models. From the resulting fingerprints of the

zero crossings locations in scale space, they observed two different classes of zero crossings:

- Stationary zero crossing locations for step and ramp edge models, and
- Nonstationary, *free* zero crossing locations for bar and staircase model, where the amount of the displacement for these zero crossing locations depend on the actual scale, whereas the direction of the displacement is governed by the relative polarity of the two concatenated step edges constituing the bar or the staircase intensity function respectively (propagation effect).

The same behavior has been also qualitatively documented for the discrete noisy 1-D case and (by simply replicating 1-D discontinuity models in a linear fashion) for the case of synthetic 2-D intensity functions.

Based upon the results of Shah et al., Piech [41] has shown how to derive the fingerprints for the ideally oriented linear 2-D step, bar, and staircase models directly from the fingerprints of the generating 1-D models. With respect to the propagation effect she demonstrated that for a given bar or staircase with width d the two constituing step edges tend to influence each other's zero crossing locations once the scale exceeds $d/3$. We will comment on this quantitative statement of Piech within the discussion of our results below.

Lu and Jain [38] drew upon Piech's findings and provided a detailed discussion on the occurrence of zero crossings of the second order derivative of Gaussian filtered bar and staircase intensity functions, including a generalization to more difficult neighbourhood contrasts. The authors again only qualitatively investigated the direction of the shift of the zero crossing with respect to the true location of the discontinuity for increasing scale.

However, Huertas and Medioni [24] also analyzed edge position accuracy for zero crossings in Laplacian of Gaussian filtered intensity functions. The authors qualitatively derived conditions for imprecision in the location of zero crossings with respect to the location of the discontinuity. For bars of width d they claimed accurate localization if $d > \omega$, where $\omega = 2\sigma$ corresponds to the diameter of central excitatory/inhibitory region of the second order derivative of a 1-D Gaussian. This seems obvious from the fact that in those cases the operator support only captures one flank of the bar leading to the simpler case of the isolated step edge discontinuity. In cases where $d < s$ (s denoting the diameter of the Gaussian convolution kernel) the locations are reported to be accurate. In case of $d < \omega$ the zero crossings are displaced by $(\omega - d)/2$. In order to overcome the localization error for bar and staircase, J.S.Chen and G. Medioni [13] proposed an iterative scheme for successive refinement of estimates for discontinuity locations. Huertas and Medioni also investigated the ramp and the roof intensity functions. For the ramp model with $d \leq s$ a zero crossing can be computed, located in the center of the ramp. For $d > s$ no reliable discontinuity localization by zero crossing detection is possible since the corresponding first derivative of this ramp will result in a plateau of certain width. The roof intensity function, where d denotes the width of one constituing ramp, causes zero crossings in the Laplacian of Gaussian operator response which are shifted with respect to the true location of the discontinuity if $d < \omega$. According to Huertas and Medioni one yields conditions as in the case of the isolated ramp for $d < \omega$ with the subconditions discussed above. We will comment on the quantitative statements of Huertas and Medioni below.

Bergholm ([5], [6]) derived a closed solution for the evaluation of zero crossing locations for bars similar to the one we derived in the preceding chapter, but lacking the compact representation with respect to a normalized scale space. The author showed numerical results for selected parameter combinations only.

This concludes our review of the most important contributions from the literature, and we want to discuss now the quantitative results which we have derived in the preceding section.

Our first investigation concentrates on the analysis of discontinuity localization for the isolated step and ramp model, respectively. We achieved the result that the localization of discontinuities always corresponds to the true location of the considered discontinuity. The scale space fingerprint for the discontinuities in both intensity functions thus is simply a straight line parallel to the axis that denotes the scale parameter.

Exceeding these two trivial cases, we also analyzed intensity functions with joint occurrence of multiple primitives, such as bar (pulse), roof, generalized bar and staircase models. These primitives have the common property to fall into the region covered by significant values of the operator kernel as scale increases, leading to mutual interference of the two discontinuities.

Figure 2 (a) shows the graph of zero crossing location $\hat{x}_{bar}$ as a function of the normalized scale parameter α. The coordinate axis, denoting the zero crossing location, is scaled with respect to the radius (half the width) R of the bar. The shape of the curve explains the qualitative observations reported within the literature cited above. One can easily recognize that the simple categorization of Huertas and Medioni [24] does not hold. The case for which $d > \omega$ and $d < \omega$ correspond to the two cases $\alpha > 1$ and $\alpha < 1$, respectively, where $d = 2R$ and $\omega = 2\sigma$. For the case of $\alpha > 1$ the zero crossing locations significantly deviate from the true point of discontinuity even in the range $1.0 < \alpha < 1.5$. This finding is in correspondence with the statement of Piech [41] that the fingerprints of adjacent discontinuities will be identical to those of the individual isolated discontinuities up to a scale of 1/3 of the distance between the two discontinuities. Using our parameters this corresponds to the range of $\alpha > 1.5$. The general solution which we have derived suggests a general trend which is in agreement with the Piech's observations. A closer look suggests a more conservative estimate since even for $\alpha \approx 1.5$ there are still visible deviations from the true discontinuity position. In additon to the graphical representation and the analytical expression the following table shows the numerical values of $\hat{x}$ for some selected α to achieve a better insight into the results.

Zero Crossing Location for Bar Function	
(True location at $\hat{x}_c = 1.0$)	
α	$\hat{x}_{bar}$
2.25	1.000
2.00	1.000
1.75	1.004
1.50	1.020
1.25	1.073
1.00	1.200
0.75	1.472
0.50	2.087
0.25	4.042

Figure 2 (b) shows the graph of the zero crossing location $\hat{x}_{roof}$ for the roof intensity function. Again, we can see that the strict categorization of Huertas and Medioni [24] is in contradiction to the result we have derived. The roof has been built by a concatenation of two ramps with opposite sign of slope. The center of the right flank of the roof (with negative slope) is located at the normalized position $\hat{x} = 0.5$. It has been stated by Huertas and Medioni that in case of $R > 2\sigma$, corresponding to $\alpha > 2$, the localization accuracy is the same as for two individual ramps. This statement suggests a constant value $\hat{x}_{roof} = 0.5$ for arguments $\alpha > 2$. This is obviously not true. Qualitatively the graph represents a monotonically increasing function of the drift of the zero crossing away from the center of the roof (i.e. $\hat{x}_{roof} = 0$) as the scale increases. Quantitative results for selected values of α are summarized in the following table to support the graphical representation.

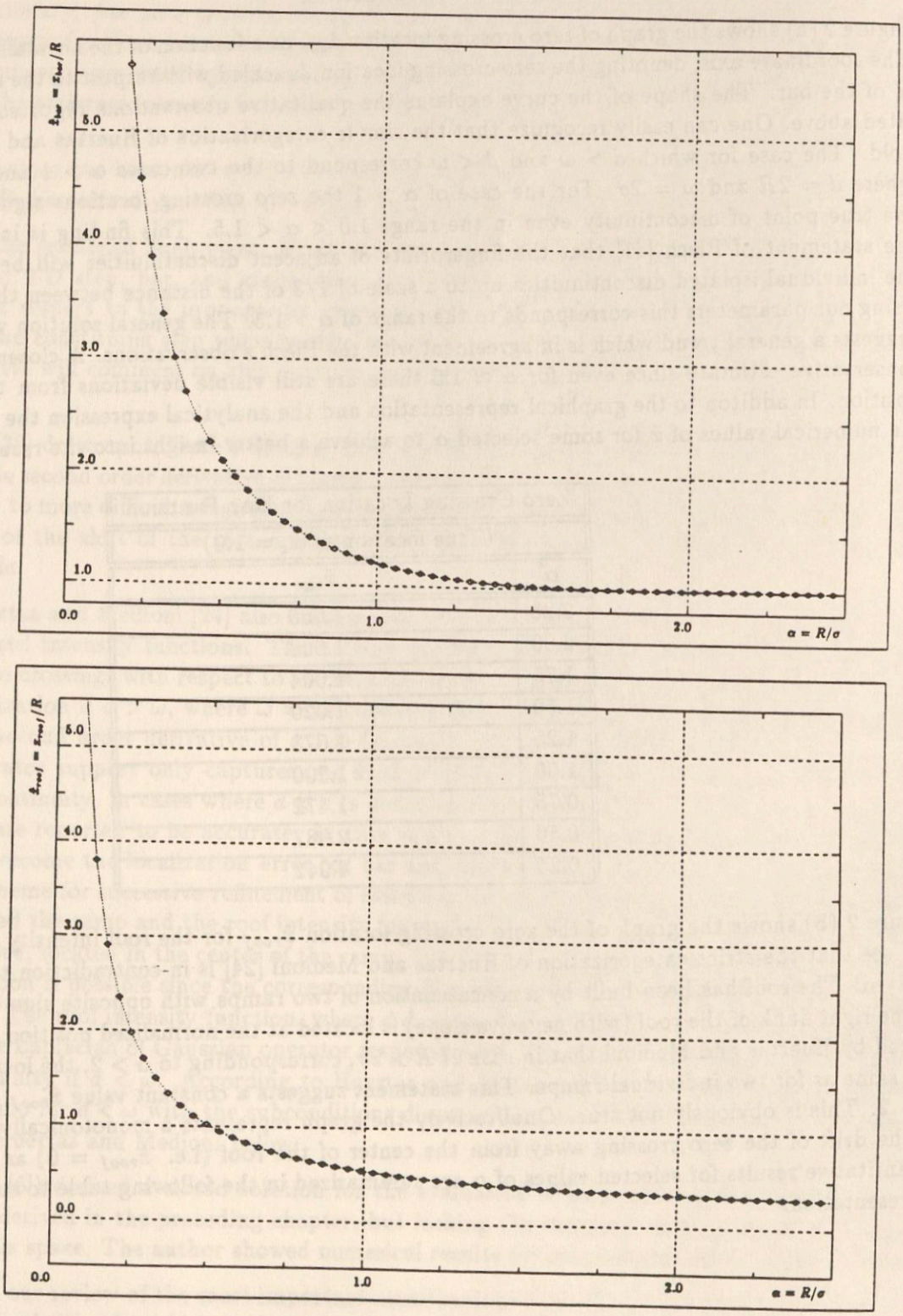

Figure 2: The graphs of the numerical solutions for the 1-D (a) bar, and (b) roof edge model

Zero Crossing Location for **Roof** Function	
(True location at $\hat{x}_c = 0.5$)	
α	$\hat{x}_{roof}$
2.25	0.318
2.00	0.336
1.75	0.361
1.50	0.398
1.25	0.454
1.00	0.543
0.75	0.698
0.50	1.021
0.25	2.010

Let us finally discuss our results on the generalized bar and the staircase model. In order to model line like intensity functions with neighbouring regions of different intensity niveaus, we have introduced - according to Piech [41] - a contrast ratio parameter a into the bar model. In case $a = 1$ we get the original bar function. Piech has shown fingerprints, i.e. scale space representations of zero crossing positions of filtered generalized bar functions, for ratios $a = 1$, $a = 2$ and $a = 8$.

Figure 3 (a) shows the graphs for the generalized bar for contrast ratios a in the interval $[0.1, 1.0]$ with step size $\Delta a = 0.1$ between the different curves. The analysis yields almost precise localization of the discontinuity for $\alpha > 2$ independent of the ratio parameter a. For scale values $\alpha < 2$ the amount of displacement of the zero crossing with respect to the true discontinuity localization increases as the value of a decreases. Figure 3 (b) provides the graphs for ratios a in the interval $[1.0, 1.9]$ with the same step size as before. The results are in accordance with the behaviour just described for Figure 3 (a). As for the bar and the roof edge the results are additionally demonstrated within the following table.

Zero Crossing Location for **Generalized Bar** Function			
(True location at $\hat{x}_c = 1.0$)			
α	$\hat{x}_{gbar}$		
	a = 0.5	a = 1.0	a= 1.5
2.25	1.000	1.000	1.000
2.00	1.001	1.000	1.000
1.75	1.008	1.004	1.002
1.50	1.038	1.020	1.014
1.25	1.126	1.073	1.051
1.00	1.327	1.200	1.145
0.75	1.761	1.472	1.344
0.50	2.851	2.087	1.762
0.25	7.649	4.042	2.780

With the introduction of the ratio a in the generalized bar function we were not only able to generate arbitrary generalized bar functions with individual neighbouring niveaus, but also - by inverting the sign of the ratio factor a - staircase models with different step heights. As an example $a = -1$ corresponds to a model with two consecutive steps with equal step height. Shah, Sood and Jain [43] as well as Lu and Jain [38] have argued on a qualitative basis that the shift of the zero crossing location for staircases

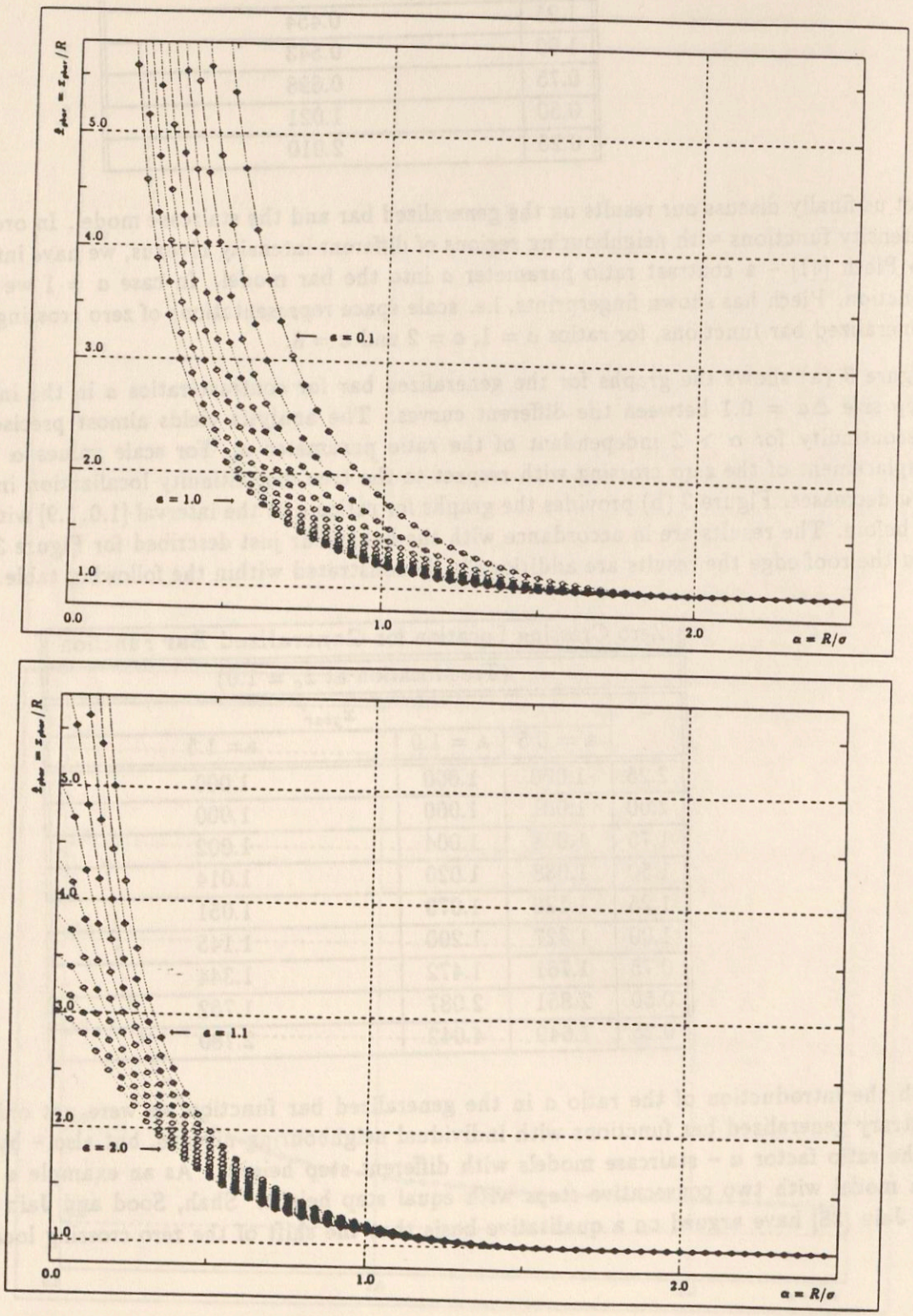

Figure 3: The graphs of the numerical solutions for the 1-D generalized bar for (a) a = 0.1 to 1.0 and for (b) a = 1.0 to 1.9

is into the opposite direction as compared to the case of a simple bar function. Within the analysis of the scale space fingerprint of such a staircase with equal step heights they demonstrate the existence of a merging point, where the locations of the zero crossings corresponding to two individual steps, merge with a third one located half the way in between the two and remain stable at this point $\hat{x}_{gbar} = 0$ as the scale further increases (see [43], Figure 8, and [14], Figure 6). Going from coarser to finer scales the zero crossing locations thus bifurcate at the merging point. The single coarse scale zero crossing is in accordance with the behaviour we have shown for the ramp edge, because the staircase can be considered as a coarsely sampled ramp edge. At the bifurcation point the individual zero crossings split into the two regular zero crossings corresponding to the two step positions, and one *phantom* zero crossing described by Clark ([14], [15]), which is due to the local minimum of the first order derivative of the low pass filtered staircase half the way in between the two flanks. In the direct surrounding of the bifurcation point one has a critical behaviour, called a *fold catastrophe* [14], in cases where the contrast ratio of the steps slightly changes from $a = 1$.

Figure 4 (a) provides the graphs of zero crossing locations for staircases according to our analysis with step contrast ratios a in the interval $[-1.0, -0.1]$ and with a stepsize of $\Delta a = 0.1$ between the different curves. The special case of $a = -1$ is easily identified as the curve that collapses from $\hat{x}_{stair} = 1.0$ down to $\hat{x}_{stair} = 0.0$. All other ratios have absolute values less than 1. With respect to Figure 1 (f) ratios $|a| < 1.0$ cause the left step to dominate over the right one. Within our numerical solutions for $\hat{x}_{stair}$ we treat $\hat{x}_{stair}$ as a function of α, so that we cannot associate more than one value with a particular α. Therefore, we derive the zero crossing locations for the minor contrast discontinuity until the scale space singularity occurs. Starting from the point of crossing over – clearly identified for each curve – we find the final part of the zero crossing locations for the dominating discontinuity of the staircase. In Figure 4 (b) the absolute values of the contrast ratio are greater than 1. The values have been taken from the interval $[-2.0, -1.1]$. The zero crossings shown in the graph correspond to the dominating step of the staircase.

The work of Piech [41] discussed above was formulated for edges separated by a distance $d = 2R$ irrespectively of the polarity of the individual edges. The finding of a critical point of mutual influence at $\alpha = 1.5$ cannot be supported from our analysis. Even for the contrast ratio $a = -1$ a significant deviation from the true location of the discontinuity can be observed. For decreasing values of a the magnitude of the shift further increases. As for the other models, numerical results for selected values of α and a are shown within the concluding table.

Zero Crossing Location for **Generalized Bar** Function (True location at $\hat{x}_c = 1.0$)			
α	$\hat{x}_{gbar}$		
	a = -0.5	a = -1.0	a= -1.5
2.25	1.000	1.000	1.000
2.00	0.999	1.001	1.001
1.75	0.991	0.996	0.997
1.50	0.945	0.975	0.984
1.25	-0.950	0.880	0.930
1.00	-0.825	0.000	0.733
0.75	-0.591	0.000	0.406
0.50	-0.424	0.000	0.262
0.25	-0.353	0.000	0.213

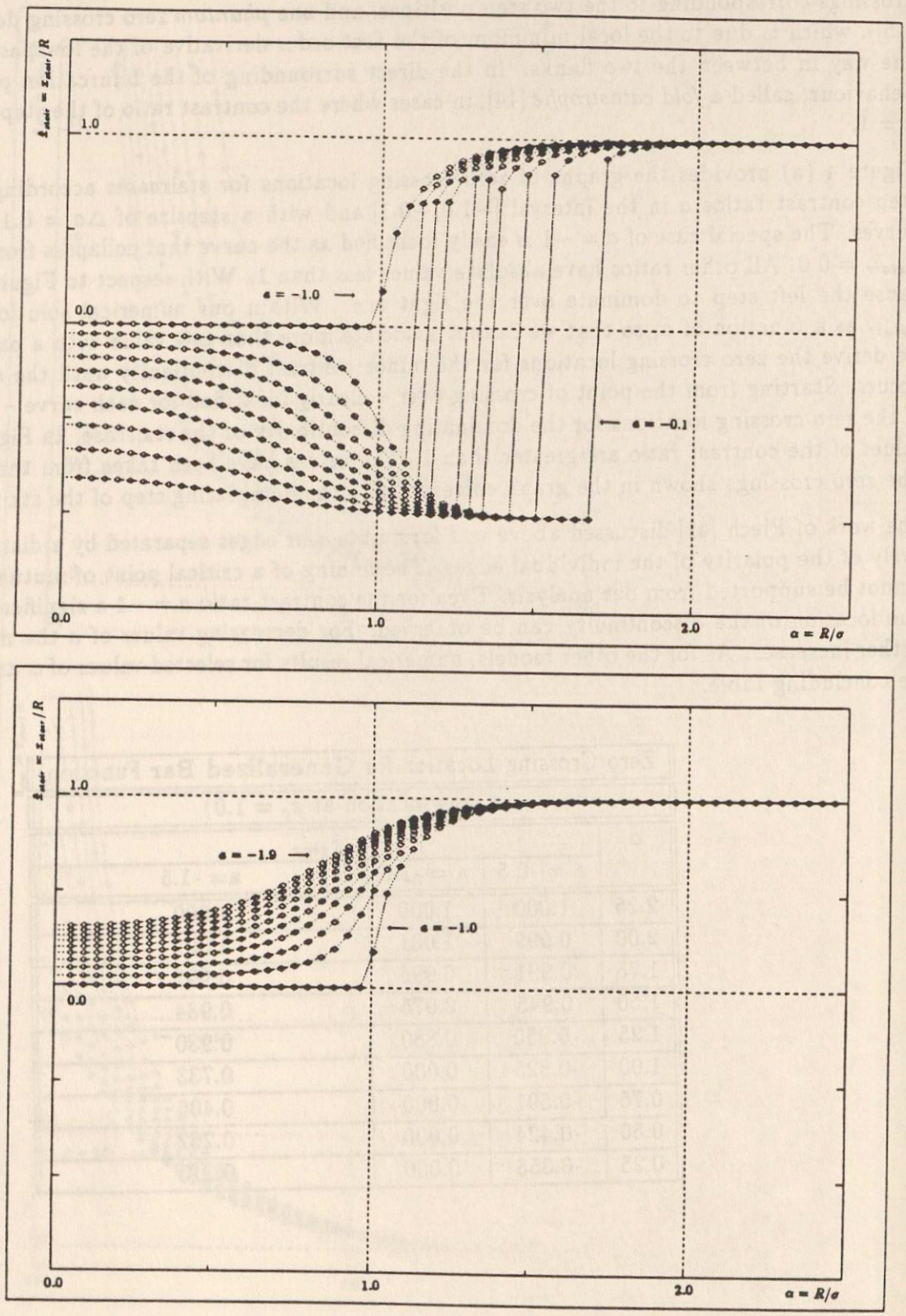

Figure 4: The graphs of the numerical solutions for the 1-D staircase model for (a) a = -0.1 to -1.0 and for (b) a = -1.1 to -2.0

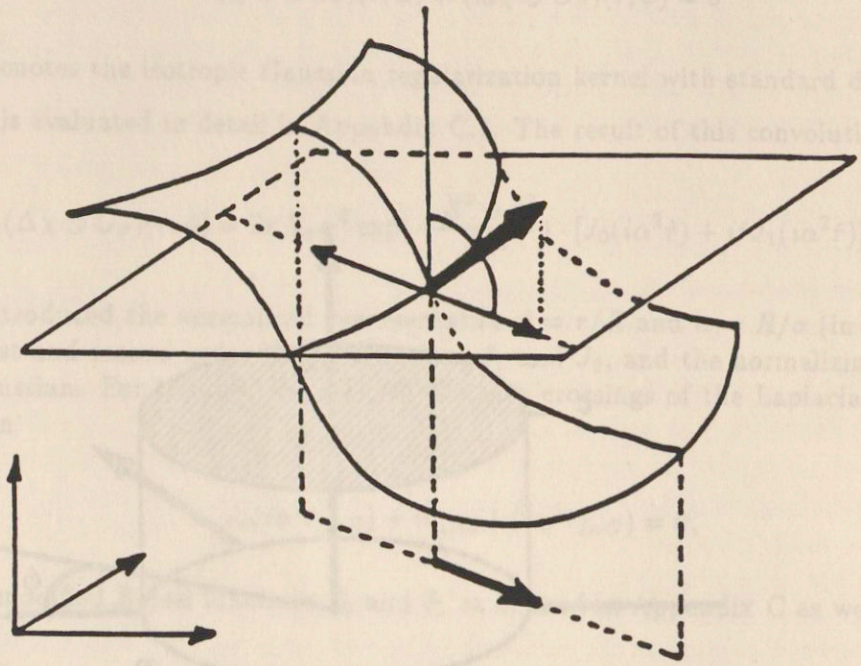

Figure 5: The local curvatures of 2-D intensity functions

3. Discontinuity Localization in 2-D Intensity Functions

3.1 A Zeroth Order Model for 2-D Intensity Functions

Assume we are given a 2-D intensity function and we look for the locations of discontinuities within the intensity function, which are defined by the locations of vanishing local curvature in the direction of the local gradient $\frac{\partial^2 f}{\partial n^2} = 0$ (for notation see Appendix B).

If our localization scheme is based on the Laplacian operator, we can derive from elementary differential geometry that the operator response of the Laplacian at points of vanishing curvature along the gradient direction is *not* zero, but

$$\Delta f|_{\frac{\partial^2 f}{\partial n^2}=0} = |\nabla f| \cdot \kappa_{isophote},$$

where $\kappa_{isophote}$ denotes the local curvature of the isophote at the position of vanishing curvature along the gradient direction (see Figure 5).

The derivation of these equation can be found in Appendix B, where we also show that

- zero crossings in Δf that coincide with $\frac{\partial^2 f}{\partial n^2}$ zero crossings are always located on intensity surface patches with local zero Gaussian curvature ($\kappa = 0$, i.e. locally flat points generated by the boundary of two parabolic patches with opposite sign of mean curvature), and
- that Δf zero crossings *not* coinciding with a $\frac{\partial^2 f}{\partial n^2}$ zero crossing are always located in a hyperbolic (intensity) surface patch, i.e. $\kappa < 0$.

In summary, zero crossings of the Laplacian operator are located either in locally flat – bounding convex and concave parabolic patches – or in hyperbolic patches. Since in general we have to deal with hyperbolic

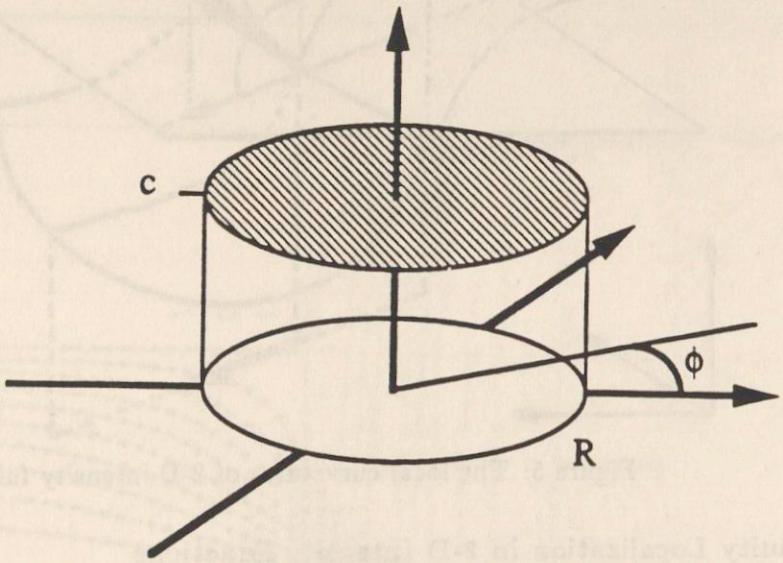

Figure 6: The zeroth order 2-D intensity model

surface patches, we will find a shift of the zero crossing of the Laplacian operator with respect to the true discontinuity location (indicated by vanishing local curvature along the gradient direction) along the direction of the local radius vector of the osculating circle.

For the purpose of quantitatively investigating this effect, we therefore define a zeroth order model of 2-D intensity functions by a Gaussian filtered cylinder, which can be independently parametrized by the radius R of the cylinder and the σ_{mod} of the Gaussian kernel. Let us initially assume $\sigma_{mod} = 0$, i.e. a crisp cylinder of radius R (see Figure 6).

This zeroth order model can be extended to higher order models by taking into account more than the constant term – represented by R – of the Fourier descriptors of the 2-D contour. For the definition of these higher order models see Appendix D.

3.2 Accuracy of Localization for the Zeroth Order 2-D Model

3.2.1 The Laplacian of Gaussian Operator

In this subsection we derive an expression for the shift of the location of the Laplacian of Gaussian zero crossing with respect to the true discontinuity location defined by the zero crossing of the second order directional derivative along the gradient of the intensity function. As we have shown above there is always a shift of the Laplacian of Gaussian zero crossing location unless the local curvature of the isophote is zero. As argued above we have chosen our zeroth order model such that this curvature is nonzero but constant:

$$\chi(r, \phi) = \mathcal{H}(R - r)$$

The location of the zero crossings of the Laplacian of Gaussian applied to this intensity function follows

from the convolution of the two functions

$$(\chi \otimes \Delta G_\sigma)(r,\phi) = (\Delta\chi \otimes G_\sigma)(r,\phi) = 0$$

where $G_\sigma(r,\phi)$ denotes the isotropic Gaussian regularization kernel with standard deviation σ.

The convolution is evaluated in detail in Appendix C.1. The result of this convolution is

$$(\Delta\chi \otimes G_\sigma)(r,\phi) = 2\pi N_\sigma \alpha^2 \exp(-\frac{R^2+r^2}{2\sigma^2}) \cdot [J_0(i\alpha^2\hat{r}) + i\hat{r}J_1(i\alpha^2\hat{r})] = 0,$$

where we have introduced the normalized representation $\hat{r} = r/R$ and $\alpha = R/\sigma$ (in correspondence to the 1-D case), the first and second order Bessel functions J_1 and J_2, and the normalizing constant N_σ for the 2-D isotropic Gaussian. For the location $\hat{r}_{LoG}$ of the zero crossings of the Laplacian of Gaussian we find from this equation

$$J_0(i\alpha^2\hat{r}_{LoG}) + i\hat{r}_{LoG}J_1(i\alpha^2\hat{r}_{LoG}) = 0,$$

which, using the modified Bessel functions I_0 and I_1 as defined in Appendix C as well, is equivalent to

$$I_0(\alpha^2\hat{r}_{LoG}) - \hat{r}_{LoG}I_1(\alpha^2\hat{r}_{LoG}) = 0. \tag{7}$$

This equation has to be solved numerically, and the result is shown in Figure 7. The result will be discussed together with the results of the first and second order directional derivatives within Section 3.3.

3.2.2 The First and Second Order Directional Derivatives of Gaussian Operators

In addition to the Laplacian of Gaussian operator investigated within the preceding section, we now derive an expression for the the first and second order directional derivatives of a Gaussian kernel to be used for discontinuity localization. Because of the rotational symmetry of our problem we can reduce our investigation to one arbitrary direction without any loss of generality. Let us thus choose the $x-$axis as the reference direction.

Looking for the maxima of the first order directional derivative along the direction of this derivative is the same as looking for the zero crossings of the second order directional derivative along this direction, for the same elementary reasons as in the 1-D case. For both discontinuity localization schemes we thus have to solve for

$$(\frac{\partial^2\chi}{\partial x^2} \otimes G_\sigma)(r,\phi) = 0,$$

resulting in (see appendix C.2 for details)

$$(\frac{\partial^2 \chi}{\partial x^2} \otimes G_\sigma)(r,\phi) =$$

$$-2\pi N_\sigma \alpha^2 \exp(-\frac{R^2+r^2}{2\sigma^2}) \cdot [\cos(2\phi) J_2(i\alpha^2 \frac{r}{R}) - J_0(i\alpha^2 \frac{r}{R}) - i(1+\cos(2\phi)) \frac{r}{R} J_1(i\alpha^2 \frac{r}{R})] = 0,$$

where we have introduced the same normalized notation as for the Laplacian of Gaussian case in the preceding subsection, and the second order Bessel function J_2.

For the location $\hat{r}_{Gxx}$ of the zero crossing of the second order directional derivative of a Gaussian kernel we find from this equation

$$\cos(2\phi) J_2(i\alpha^2 \hat{r}_{Gxx}) - J_0(i\alpha^2 \hat{r}_{Gxx}) - i(1+\cos(2\phi)) \hat{r}_{Gxx} J_1(i\alpha^2 \hat{r}_{Gxx}) = 0,$$

which, using the modified Bessel functions I (see Appendix C) instead of J, is equivalent to

$$I_0(\alpha^2 \hat{r}_{Gxx}) + \cos(2\phi) I_2(\alpha^2 \hat{r}_{Gxx}) - (1+\cos(2\phi)) \hat{r}_{Gxx} I_1(\alpha^2 \hat{r}_{Gxx}) = 0.$$

As in the case of the Laplacian of Gaussian, this equation has to be solved numerically. The result is shown in Figure 9, and will be discussed together with the results from the Laplacian of Gaussian in the following section.

3.3 Discussion of Results

In a large number of publications on edge localization in 2-D intensity functions, the displacement of the detected location of a discontinuity with respect to the true location, indicated by the zero crossing of the second order directional derivative along the local gradient direction, has been discussed.

Based upon early work of Abdou and Pratt [1], Kitchen and Malin [26] published an analytical study of classical discontinuity localization schemes - such as proposed by Sobel, Prewitt and Roberts - with respect to their magnitude and directional response. The model underlying Kitchen and Malin's analysis assumes an infinite straight unit step edge, with an orientation between 0 and 45 degrees with respect to the ordinate, passing through a unit square pixel in a noise-free discrete image. This unit square pixel is also considered the center of the convolution mask. The result of this thorough investigation sets limits to the performance that can be expected from these conventional simple discontinuity localization schemes.

Beyond this type of investigations by simply extending 1-D concepts into 2-D (see the discussions within subsection 2.3 on the results of the 1-D cases), mainly the Laplacian operator applied to Gaussian filtered intensity functions has been analyzed in more detail by Clark [14], Berzins [7], Bergholm [6] and Lei [36] with respect to the intrinsic 2-D problems caused by differential geometry of 2-D intensity surfaces (see also [32] and, in particular, the detailed analysis in [45]).

Clark not only investigated the Laplacian operator on the basis of the local differential geometry of the intensity surface, but also observed resulting phantom edges due to the involved zero crossing method. Similar to our analysis Clark showed that zero crossings of $\frac{\partial^2 f}{\partial n^2}$ not necessarily coincide with zero crossings of the Laplacian operator. However, a qualitative estimation of this effect was not within the scope of his paper. Such a qualtitative analysis was done by Bergholm within his thesis on the information of edges

and optical flow. Herein, Bergholm [6] described *rounding-off* and *expansion* effects of the discontinuity contours based on the Laplacian of Gaussian operator.

In contrast to this qualitative analysis of the discontinuity localization of Laplacian of Gaussian schemes, only a few quantitative investigations can be reported. At first, Berzins [7] analysed in detail the rounding-off effect for perfect V-junctions, built by a predefined angle α, assuming infinite extension of the structure, or at least a large extent compared to the standard deviation of the regularizing Gaussian kernel.

An approach most similar to ours was published by Lei [36] in 1988. In a theoretical paper Lei extended Spacek's [44] contribution to solely local curvature measurement, based on an analysis of the level-crossings curvature of a special type of intensity function. In reducing the degrees of freedom of the model for the underlying intensity function by a coupling of the local contrast to the scale of the discontinuity, Lei derived an analytic expression for the shift of the zero crossing location of the Laplacian operator with respect to the true location. This shift was shown to be proportional both to the local gradient magnitude at the position R of the true discontinuity and to a function of the ratio between σ and R, which we have introduced as α in our analysis. In addition to the loss of generality with respect to the intensity function model, Lei's solution also does not show the full scaling property with respect to the model blurring parameter σ as described below. The numerical solutions of our result on the Laplacian of Gaussian for the unblurred cylinder model are shown in Figure 7 (a) and Figure 7 (b). While Figure 7 (a) has a linear scaling on both axes, Figure 7 (b) has a logarithmic scaling of the zero crossing coordinate. It can bee seen from the two figures that the relative error of the location of the Laplacian of Gaussian zero crossing with respect to the radius R of the cylinder is a strongly decreasing function of the ratio α between R and the standard deviation σ_{reg} of the regularizing Gaussian. Indeed this decay is stronger than exponential as can be seen in Figure 7 (b), where the zero crossing coordinate has been scaled logarithmically. This behaviour is precisely what one intuitively expects due to the fact that an increasing α (corresponding to a decreasing σ_{reg} for fixed R) leads to an increasing straightness of the contour of the cylinder on a spatial scale compared to σ_{reg}. Thus to the operator, the contour looks more and more like a halfplane step edge, which is the generalization of the 1-D step edge to 2-D. As we have derived in chapter 2, the localization of the zero crossing of the second order derivative corresponds to the true location of the discontinuity. Thus the zero crossing of the Laplacian of Gaussian in 2-D is expected to converge asymptotically to the location of the cylinder discontinuity. From Figures 7a and 7b it can bee seen as well that there is no *real* critical point of the scheme, i.e. a point α where a substantial change of the underlying effects can be observed. One generally is attracted to interpret some points of such a graph as being more important than the others. However, often those points are closer related to the characteristics of graphical representation alone than to an effect of the underlying problem. The Figures should thus be understood as characteristic curves of the Laplacian of Gaussian operator applied to 2-D intensity function with locally constant curvature. In combination with the selection of a Gaussian filter for regularization of discontinuity localization, which always tends to increase the standard deviation of the Gaussian to achieve a sufficient smoothing capability, the intrinsic localization error of the Laplacian operator on image structures of arbitrary size can be either estimated from the characteristic curve or derived from the underlying equation. In Figure 8 we show a graph corresponding to the shifted lines of zero crossings for values of α between $\alpha = 0.2$ and $\alpha = 4.0$.

Within the discussion of Lei's results we mentioned the full scaling property of our result. The equations for the zero crossing locations derived in this chapter always correspond to the case of a crisp cylinder. Our zeroth order model on the other hand allows arbitrary Gaussian blurring of the crisp cylinder to yield arbitrarily scaled discontinuities. As for the 1-D case we simply have to rescale α by replacing σ_{reg} in the nominator of α by $\sigma_{eff} = \sqrt{\sigma_{reg}^2 + \sigma_{mod}^2}$, i.e. rescaling α to $\tilde{\alpha} = (\sigma_{reg}/\sigma_{eff}) \cdot \alpha$. In order to complete the graphical and analytical results by some numerical values of $\tilde{r}$ for selected values of α we calculated the following table.

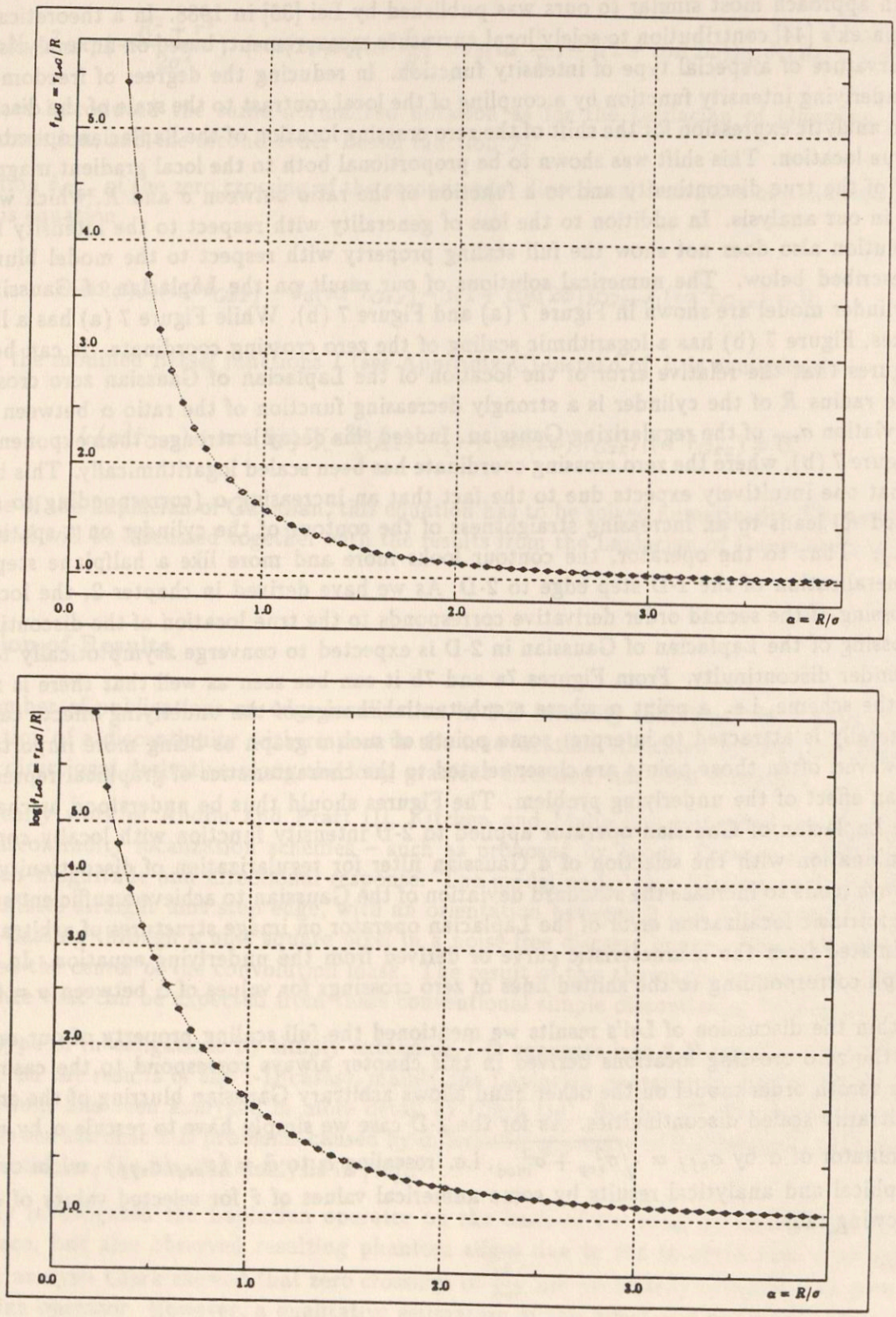

Figure 7: The graphs of the numerical solutions for the Laplacian of Gaussian with (a) linear scaling of both axes, and (b) logarithmic scaling of the coordinate axis.

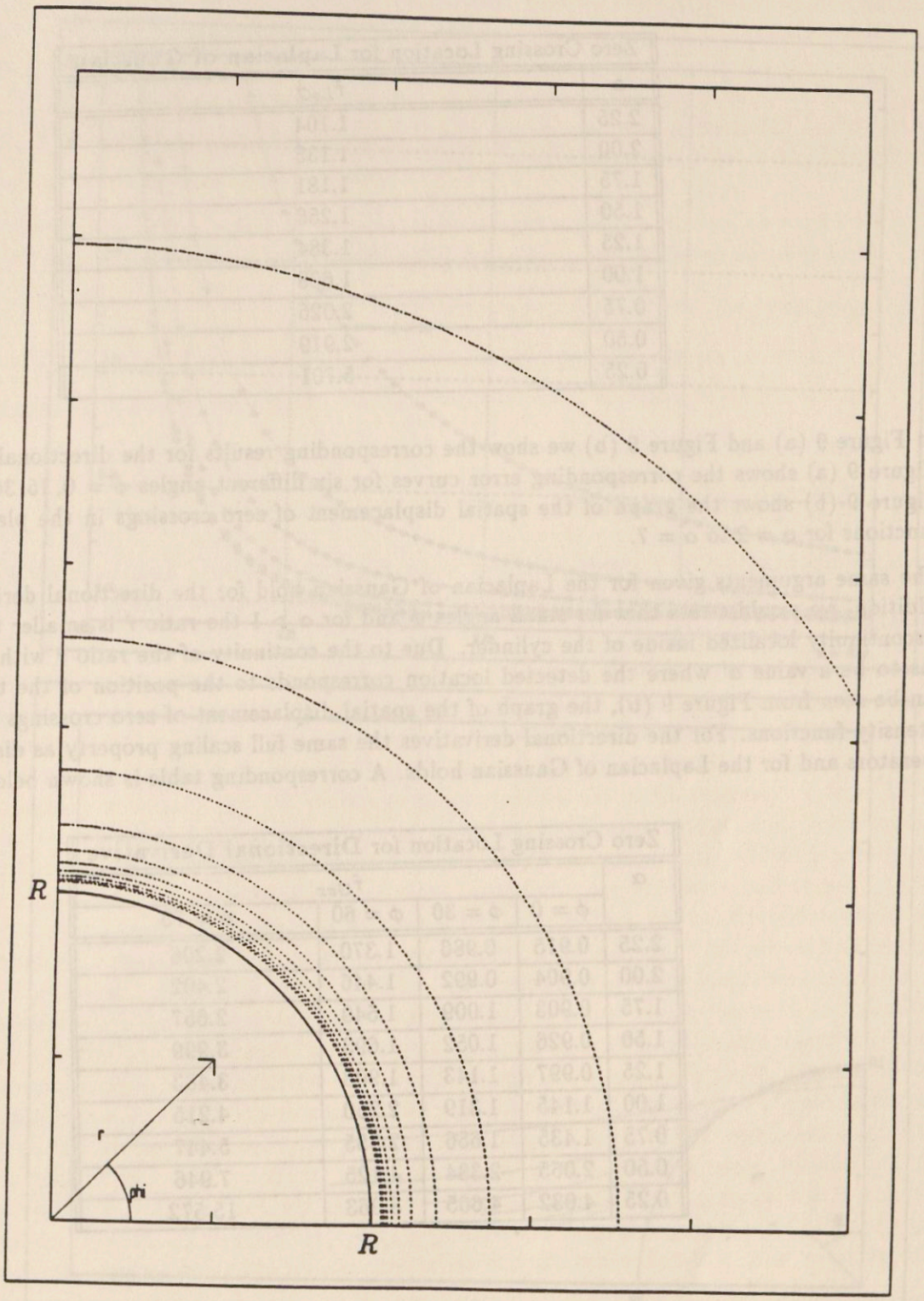

Figure 8: Lines of zero crossings of the Laplacian of Gaussian for α from 0.2 to 4.0

Zero Crossing Location for **Laplacian of Gaussian**	
α	$\hat{r}_{LoG}$
2.25	1.104
2.00	1.135
1.75	1.181
1.50	1.256
1.25	1.384
1.00	1.608
0.75	2.026
0.50	2.919
0.25	5.701

In Figure 9 (a) and Figure 9 (b) we show the corresponding results for the directional derivatives. While Figure 9 (a) shows the corresponding error curves for six different angles $\phi = 0, 15, 30, 45, 60, 75$ degrees, Figure 9 (b) shows the graph of the spatial displacement of zero crossings in the plane of the intensity functions for $\alpha = 2$ to $\alpha = 7$.

The same arguments given for the Laplacian of Gaussian hold for the directional derivatives as well. In addition, we would stress that for small angles ϕ and for $\alpha > 1$ the ratio $\hat{r}$ is smaller than 1 leading to a discontinuity localized inside of the cylinder. Due to the continuity of the ratio $\hat{r}$ with respect to α there has to be a value α' where the detected location corresponds to the position of the true location. This can be seen from Figure 9 (b), the graph of the spatial displacement of zero crossings in the plane of the intensity functions. For the directional derivatives the same full scaling property as discussed for the 1-D operators and for the Laplacian of Gaussian holds. A corresponding table is shown below.

Zero Crossing Location for **Directional Derivative**				
α	$\hat{r}_{Gxx}$			
	$\phi = 0$	$\phi = 30$	$\phi = 60$	$\phi = 75$
2.25	0.915	0.986	1.370	2.206
2.00	0.904	0.992	1.446	2.402
1.75	0.903	1.009	1.549	2.657
1.50	0.926	1.052	1.693	3.999
1.25	0.997	1.143	1.908	3.483
1.00	1.145	1.319	2.250	4.215
0.75	1.435	1.656	2.855	5.447
0.50	2.065	2.384	4.125	7.946
0.25	4.032	4.665	8.063	15.572

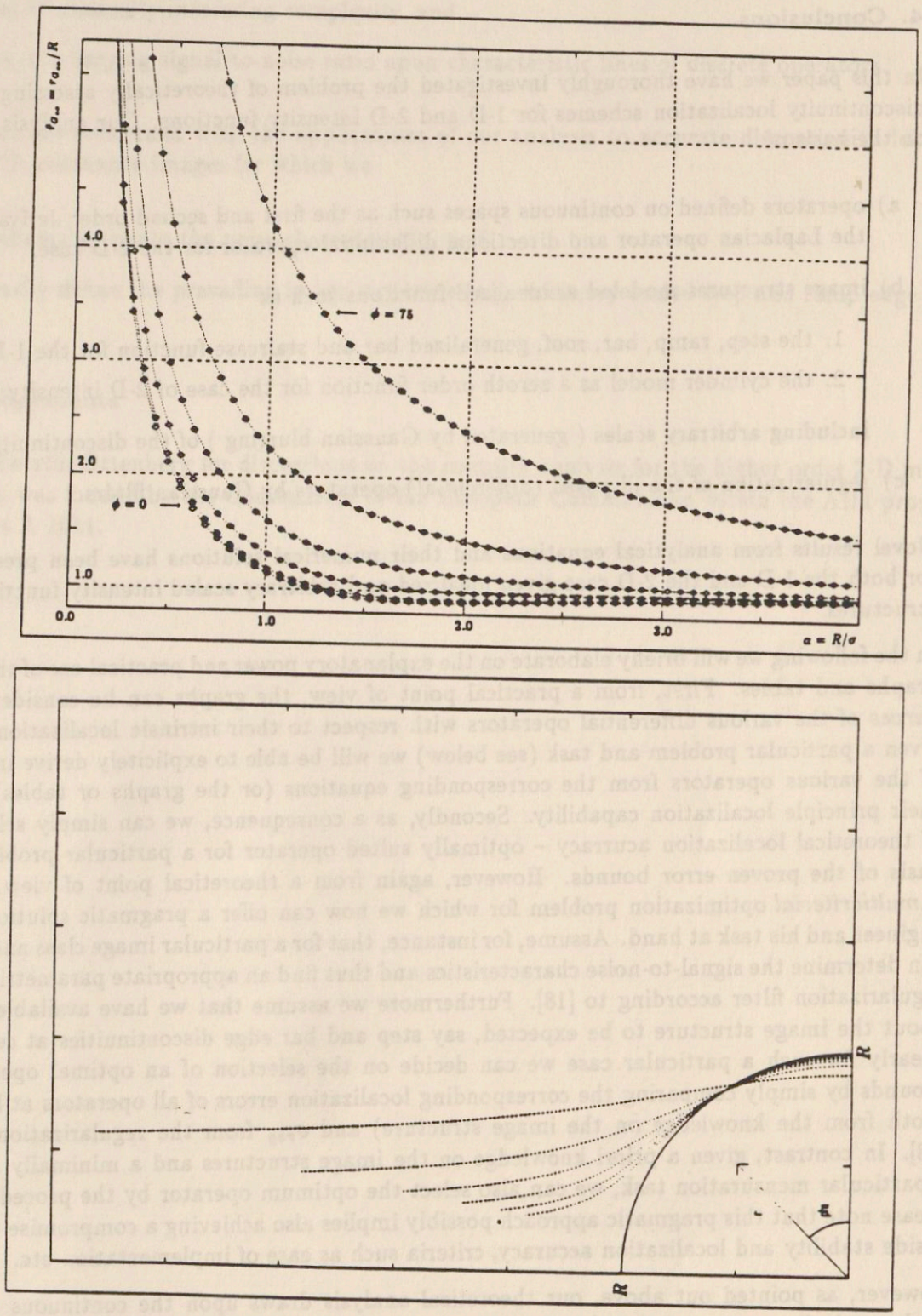

Figure 9: The graphs of the numerical solutions for the directional derivatives (a) for angles $\phi =$ 0, 15, 30, 45, 60, 75 degree, and (b) the spatial plot of the locations of discontinuities for α between 0.3 and 4.0

4. Conclusions

In this paper we have thoroughly investigated the problem of theoretically assessing the intrinsic error of discontinuity localization schemes for 1-D and 2-D intensity functions. Our analysis has been carried out on the basis of

a) operators defined on continuous spaces such as the first and second order derivative for the 1-D case, the Laplacian operator and directional differential operator for the 2-D case,

b) image structures modeled as idealized functions such as

   1. the step, ramp, bar, roof, generalized bar and staircase function for the 1-D case,
   2. the cylinder model as a zeroth order function for the case of 2-D intensity functions,

   including arbitrary scales (generated by Gaussian blurring) of the discontinuities for both cases,

c) regularization of the ill-posed (differential) operators by Gaussian filters.

Novel results from analytical equations and their numerical solutions have been presented and discussed for both the 1-D and the 2-D case given idealized and arbitrary scaled intensity functions modelling image structures.

In the following we will briefly elaborate on the explanatory power and practical use of the resulting formulas, graphs and tables. First, from a practical point of view, the graphs can be considered as *characteristic curves* of the various differential operators with respect to their intrinsic localization capabilities. Thus, given a particular problem and task (see below) we will be able to explicitely derive intrinsic error bounds of the various operators from the corresponding equations (or the graphs or tables) such as to predict their principle localization capability. Secondly, as a consequence, we can simply select the – in a sense of theoretical localization acurracy – optimally suited operator for a particular problem and task on the basis of the proven error bounds. However, again from a theoretical point of view, such a selection is a *multicriterial* optimization problem for which we now can offer a pragmatic solution useful e.g. for an engineer and his task at hand. Assume, for instance, that for a particular image class and imaging device, we can determine the signal-to-noise characteristics and thus find an appropriate parametrization of a Gaussain regularization filter according to [18]. Furthermore we assume that we have available a priori knowledge about the image structure to be expected, say step and bar edge discontinuities at certain spatial scales. Clearly for such a particular case we can decide on the selection of an optimal operator on theoretical grounds by simply comparing the corresponding localization errors of all operators at hand, given R, σ_{mod} (both from the knowledge on the image structure) and σ_{reg} from the regularization filter according to [18]. In contrast, given a priori knowledge on the image structures and a minimally acceptable error for a particular mensuration task, we can also select the optimum operator by the procedure sketched above. Please note that this pragmatic approach possibly implies also achieving a compromise taking into account, beside stability and localization accuracy, criteria such as ease of implementation etc..

However, as pointed out above, our theoretical analysis draws upon the continuous case only, resulting in theoretically proven inherent error bounds. Consequently, in the future we will further investigate the problems related to the discrete case, i.e.

a) effects of quantization and sampling of the image intensity function and the operators upon the characteristic curves,

b) determination of characteristic lines of various discrete operators as applied to, for instance, synthetic images of gradually increasing complexity, and

c) effects of a varying signal-to-noise ratio upon characteristic lines of discrete operators.

Moreover we are concerned with the applications of our analysis to accurate discontinuity localization in e.g. magnetic resonance images for which we

a) can reliably estimate the noise characteristic, and

b) can easily define the prevailing image structure (e.g. arbitrary scaled step and ramp edge discontinuities).

Acknowledgements

We thank Kerstin Ottenberg for discussions on the complex analysis for the higher order 2-D models. Part of this work was funded by the Commission of the European Communities within the AIM program under the contract A 1011.

Appendix A: Derivation of Equations for 1-D Intensity Functions

A.1 Step edge

The 1-D intensity function for the step edge located at position $x = Z$ having local contrast c is defined to be

$$f_{step}(x) = c \cdot \mathcal{H}(x - Z)$$

where $\mathcal{H}$ denotes the Heaviside function defined as[1]

$$\mathcal{H}(x) = \begin{cases} 0 & \text{if } x < 0 \\ 1 & \text{if } x \geq 0 \end{cases}$$

The second order derivative of the Gaussian filtered function f_{step} yields

$$\frac{\partial^2 (c \cdot \mathcal{H}(x - Z) \otimes G_\sigma(x))}{\partial x^2} = c \cdot \delta'(x - Z) \otimes G_\sigma(x).$$

Using the derivative sifting property of the unit impulse ([9]), the convolution of the derivative of the delta function – defined in the common sense of distributions – shifted by Z with the Gaussian, yields the first order derivative of this Gaussian centered at location Z. The zero crossing of this function determines the localization point of the discontinuity for the filtered step edge model to be

$$-\frac{c \cdot (x_{step} - Z)}{\sqrt{2\pi} \cdot \sigma^3} \cdot \exp[\frac{-(x_{step} - Z)^2}{(2\sigma^2)}] = 0,$$

i.e.

$$x_{step} = Z.$$

A.2 Ramp edge

We define the function for the ramp discontinuity by using a rectangular function $\Pi(\frac{x}{2Z}) = \mathcal{H}(x + Z) - \mathcal{H}(x - Z)$ (the difference between two shifted Heaviside functions) which is convolved with a Heaviside function. Without loss of generality, the function Π can be assumed as centered at the origin. The resulting intensity function f_{ramp} has therefore positive slope within the interval $[-Z, Z]$:

$$f_{ramp}(x) = c \cdot (\Pi(\frac{x}{2Z}) \otimes \mathcal{H}(x)).$$

The second order derivative of the Gaussian filtered function f_{ramp} yields

[1] In the literature, e.g. [9], [40], [39], we find several distinct definitions for the Heaviside function with respect to the functional value at location $x = 0$. The notation for the Heaviside function we use here is the one of [39].

$$\frac{\partial^2(c \cdot (\Pi(\frac{x}{2Z}) \otimes \mathcal{H}(x)) \otimes G_\sigma(x))}{\partial x^2} = c \cdot (\delta(x+Z) - \delta(x-Z)) \otimes G_\sigma(x).$$

Since the convolution is a linear operation, the sum of the two delta functions can be treated separately. The estimated localization x_{ramp} of the discontinuity is found at the zero crossing of the above equation. Thus, we have to solve

$$c \cdot (G_\sigma(x_{ramp} + R) - G_\sigma(x_{ramp} - R)) = 0.$$

This is equivalent to

$$\frac{c}{\sqrt{2\pi} \cdot \sigma} \cdot [\exp(\frac{-(x_{ramp}+R)^2}{(2\sigma^2)}) - \exp(\frac{-(x_{ramp}-R)^2}{(2\sigma^2)})] = 0$$

After the separation of the components we get

$$\exp(\frac{-x_{ramp}^2}{2\sigma^2}) \cdot \exp(\frac{-R \cdot x_{ramp}}{\sigma^2}) \cdot \exp(\frac{-R^2}{2\sigma^2}) = \exp(\frac{-x_{ramp}^2}{2\sigma^2}) \cdot \exp(\frac{R \cdot x_{ramp}}{\sigma^2}) \cdot \exp(\frac{-R^2}{2\sigma^2})$$

and finally

$$\exp(\frac{2R \cdot x_{ramp}}{\sigma^2}) = 1.$$

Therefore, the discontinuity of the ramp transition as defined above is always located at

$$x_{ramp} = 0. \quad \square$$

A.3 Bar (Pulse) primitive

As defined in A.2, a rectangular intensity variation that models a bar can be described as the difference of two shifted Heaviside functions. Without loss of generality, we defined the bar to be centered at the origin, therefore the two flanks are located at $-R$ and R, respectively. The bar function is then defined by

$$f_{bar}(x) = c \cdot \Pi(\frac{x}{2R}),$$

and the second order derivative of the Gaussian filtered function f_{bar} gives

$$\frac{\partial^2(c \cdot \Pi(\frac{x}{2R}) \otimes G_\sigma(x))}{\partial x^2} = c \cdot [\delta'(x+R) - \delta'(x-R)] \otimes G_\sigma(x).$$

As expected, this result reflects the fact that a bar function can be considered as the first derivative of a ramp. Therefore, the next steps in the derivation are straightforward: The zero crossing of the function are found at

$$\frac{c}{\sqrt{2\pi}\cdot\sigma^3}\cdot[(x_{bar}-R)\cdot\exp(\frac{-(x_{bar}-R)^2}{2\sigma^2})-(x_{bar}+R)\cdot\exp(\frac{-(x_{bar}+R)^2}{2\sigma^2})]=0$$

which is equivalent to

$$x_{bar}\cdot[\exp(\frac{-(x_{bar}-R)^2}{2\sigma^2})-\exp(\frac{-(x_{bar}+R)^2}{2\sigma^2})]=R\cdot[\exp(\frac{-(x_{bar}-R)^2}{2\sigma^2})+\exp(\frac{-(x_{bar}+R)^2}{2\sigma^2})].$$

We now replace the variable x_{bar} by $\hat{x}_{bar}$ (which is scaled with respect to the radius R of the bar function (see Section 2.2), $\hat{x}_{bar}=x_{bar}/R$). The above equation thus reduces to

$$(\hat{x}_{bar}-1)\cdot\exp(\frac{-(x_{bar}-R)^2}{2\sigma^2})=(\hat{x}_{bar}+1)\cdot\exp(\frac{-(x_{bar}+R)^2}{2\sigma^2})$$

and further to

$$(\hat{x}_{bar}-1)\cdot\exp(\frac{2R\cdot x_{bar}}{\sigma^2})=\hat{x}_{bar}+1.$$

In order to get unified results, we further introduce the variable $\alpha=R/\sigma$ as described in Section 2.2, which leads to

$$\exp(2\alpha^2\cdot\hat{x}_{bar})+1-\hat{x}_{bar}\cdot[\exp(2\alpha^2\cdot\hat{x}_{bar})-1]=0.$$

Multiplying this equation with $\exp(-\alpha^2\cdot\hat{x}_{bar})$ and using the identities $\cosh(x)=\frac{1}{2}[\exp(x)+\exp(-x)]$ and $\sinh(x)=\frac{1}{2}[\exp(x)-\exp(-x)]$ we finally get

$$\cosh(\alpha^2\cdot\hat{x}_{bar})-\hat{x}_{bar}\cdot\sinh(\alpha^2\cdot\hat{x}_{bar})=0$$

or, equivalently,

$$\hat{x}_{bar}\cdot\tanh(\alpha^2\cdot\hat{x}_{bar})=1.$$

A.4 Roof primitive

A roof shaped intensity function Λ can be precisely described by the self convolution of a bar function, i.e. $\Lambda(\frac{x}{R})=\Pi(\frac{x}{R})\otimes\Pi(\frac{x}{R})$. If the bar is centered at the origin, the roof is located at the same location extending over the interval $[-R,R]$. The function f_{roof} with slope of the two flanks equal to $|c/R|$ is given by

$$f_{roof}(x)=c\cdot\Pi(\frac{x}{R})\otimes\Pi(\frac{x}{R}).$$

The second order derivative of the Gaussian filtered function is

$$\frac{\partial^2(c\cdot(\Pi(\frac{x}{R})\otimes\Pi(\frac{x}{R}))\otimes G_\sigma(x))}{\partial x^2} = \frac{\partial(c\cdot((\delta(x+\frac{1}{2}R)-\delta(x-\frac{1}{2}R))\otimes(\mathcal{H}(x+\frac{1}{2}R)-\mathcal{H}(x-\frac{1}{2}R)))\otimes G_\sigma(x))}{\partial x}$$

Separating the first convolution of the right hand side from the other ones and using Fourier's shift theorem we yield the simple result

$$c\cdot(\delta(x+\frac{1}{2}R)-\delta(x-\frac{1}{2}R))\otimes(\mathcal{H}(x+\frac{1}{2}R)-\mathcal{H}(x-\frac{1}{2}R)) = c\cdot(\mathcal{H}(x+R)-2\mathcal{H}(x)+\mathcal{H}(x-R)).$$

The second order derivative of the Gaussian filtered roof then yields

$$\frac{\partial^2(f_{roof}(x)\otimes G_\sigma(x))}{\partial x^2} = c\cdot(\delta(x+R)-2\delta(x)+\delta(x-R))\otimes G_\sigma(x).$$

For the evaluation of the localization accuracy, we again have to determine the zero crossing of this function. The convolution of the Gaussian with a sequence of delta functions results in replicated Gaussians located at the positions of the deltas. We thus get for x_{roof} :

$$\frac{c}{\sqrt{2\pi}\cdot\sigma}\cdot[\exp(\frac{-(x_{roof}+R)^2}{2\sigma^2})-2\cdot\exp(\frac{-x_{roof}^2}{2\sigma^2})+\exp(\frac{-(x_{roof}-R)^2}{2\sigma^2})] = 0.$$

The term $\exp(-x_{roof}^2/2\sigma^2)$ can be eliminated from the equation and we replace x, R and σ by the scaled parameters $\hat{x}$ and α yielding

$$[\exp(-\alpha^2\cdot\hat{x}_{roof})+\exp(\alpha^2\cdot\hat{x}_{roof})]\cdot\exp(-\frac{1}{2}\alpha^2) = 2.$$

Introducing the hyperbolic cosine as in Appendix A.3 we yield

$$\alpha^2\cdot\hat{x}_{roof} = \operatorname{arcosh}[\exp(\frac{1}{2}\alpha)].$$

Using the identity $\operatorname{arcosh}(x) = \ln(x\pm\sqrt{x^2-1})$ finally yields an analytical expression for the zero crossing location $\hat{x}_{roof}$

$$\hat{x}_{roof} = \frac{1}{\alpha^2}\cdot\ln[\exp(\frac{\alpha^2}{2})+\sqrt{\exp(\alpha^2)-1}].$$

A.5 Generalized Bar (Pulse) and Staircase function

In A.3 the (simple) bar primitive was defined as the difference of two shifted Heaviside functions, both with contrast c, located at $-R$ and R, respectively. By introduction of a contrast ratio a, as described in Section 2.2, different contrasts of the two constituing steps are allowed, the second step height related to the first by the factor a. The generalized bar function is therefore defined as

$$f_{gbar}(x) = c \cdot [\mathcal{H}(x+R) - a \cdot \mathcal{H}(x-R)],$$

and the second order derivative of the Gaussian filtered function f_{gbar} yields

$$\frac{\partial^2 (c \cdot (\mathcal{H}(x+R) - a \cdot \mathcal{H}(x-R)) \otimes G_\sigma(x))}{\partial x^2} = c \cdot [\delta'(x+R) - a \cdot \delta'(x-R)] \otimes G_\sigma(x).$$

Using the intermediate results of the derivations for the simple bar, and again introducing the normalized scaling parameters $\hat{x}$ and α, we derive the corresponding intermediate result for zero point location of the generalized bar $\hat{x}_{gbar}$:

$$a \cdot \exp(2\alpha^2 \cdot \hat{x}_{gbar}) + 1 - \hat{x}_{gbar} \cdot [a \cdot \exp(2\alpha^2 \cdot \hat{x}_{gbar}) - 1] = 0,$$

or equivalently

$$[a \cdot \exp(\alpha^2 \cdot \hat{x}_{gbar}) + \exp(-\alpha^2 \cdot \hat{x}_{gbar})] - \hat{x}_{gbar} \cdot [a \cdot \exp(\alpha^2 \cdot \hat{x}_{gbar}) - \exp(-\alpha^2 \cdot \hat{x}_{gbar})] = 0.$$

Using the hyperbolic sine and cosine introduced in Appendix A.3 we get the final result for the location of the zero crossing for the generalized bar as

$$[(a+1) \cdot \cosh(\alpha^2 \cdot \hat{x}_{gbar}) + (a-1) \cdot \sinh(\alpha^2 \cdot \hat{x}_{gbar})] - \hat{x}_{gbar} \cdot [(a-1) \cdot \cosh(\alpha^2 \cdot \hat{x}_{gbar}) + (a+1) \cdot \sinh(\alpha^2 \cdot \hat{x}_{gbar})] = 0.$$

For $a = 1$ this equation reduces to $\cosh(\alpha^2 \cdot \hat{x}) - \hat{x} \cdot \sinh(\alpha^2 \cdot \hat{x}) = 0$, representing the equation we derived for the simple bar.

The intensity function of staircases, being a combination of steps of equal polarities, can be considered as a special type of the generalized bar, where the ratio factor a is negative. Therefore, we can use the above equation for the determination of zero crossing locations of the second order derivative of differently parametrized staircases. For convenience, in order to parametrize with positive values for a, the equation has been rewritten. Straightforwardly, we get

$$\hat{x}_{stair} \cdot [a \cdot \exp(\alpha^2 \cdot \hat{x}_{stair}) + \exp(-\alpha^2 \cdot \hat{x}_{stair})] - [a \cdot \exp(\alpha^2 \cdot \hat{x}_{stair}) - \exp(-\alpha^2 \cdot \hat{x}_{stair})] = 0.$$

corresponding to

$$[(1-a) \cdot \cosh(\alpha^2 \cdot \hat{x}_{stair}) - (1+a) \cdot \sinh(\alpha^2 \cdot \hat{x}_{stair})] + \hat{x}_{stair} \cdot [(1+a) \cdot \cosh(\alpha^2 \cdot \hat{x}_{stair}) - (1-a) \cdot \sinh(\alpha^2 \cdot \hat{x}_{stair})] = 0.$$

Appendix B: Elements of Differential Geometry for 2-D Intensity Functions

This appendix contains some elements of differential geometry as they are of interest to the localization of 2-D discontinuities. The necessity of introducing differential geometry becomes obvious from the attempt to describe the problem of discontinuity localization in terms of the local characteristic of the intensity function. This approach generally leads to a change of the coordinate system from the cartesian coordinates $(x_i)_{i=1..N}$ to a curved coordinate system $(u_i)_{i=1..N}$, related to the problem under consideration, such that every point $\vec{r}$ can be described by the corresponding x or u coordinate values respectively.

Along the tangents of the curves $u_i = const.$ we define a local system of unit vectors $\vec{e}_{u_i}$ by normalizing the tangent vectors:

$$\vec{e}_{u_i} = \frac{\partial \vec{r}}{\partial u_i} \cdot [\| \frac{\partial \vec{r}}{\partial u_i} \|]^{-1}$$

Related to each coordinate system we further define entities characteristically for this coordinate sysytem, which allow the formulation of a problem entirely in terms of these entities, so that the *form* of the resulting equations becomes independent of the underlying coordinate system. The entities to be introduced for our purposes are the *metric tensor* g_{ij} and the *Christoffelsymbols* Γ^k_{ij} defined as:

$$\begin{aligned} g_{ij} &= \frac{\partial \vec{r}}{\partial u_i} \cdot \frac{\partial \vec{r}}{\partial u_j} \\ \Gamma^k_{ij} &= \frac{1}{2} g^{kl} [\frac{\partial g_{il}}{\partial u^j} + \frac{\partial g_{jl}}{\partial u^i} - \frac{\partial g_{ij}}{\partial u^l}], \end{aligned}$$

where we have used the Einstein convention for automatic summation over indices occurring twice.

Using these definitions we can write the Laplacian operator for arbitrary coordinate systems as

$$\begin{aligned} \Delta &= \frac{\partial}{\partial u^i} [g^{ij} \frac{\partial}{\partial u^i}] + \Gamma^k_{ik} g^{ij} \frac{\partial}{\partial u^j} \\ &= \frac{\partial^2}{\partial u^i \partial u^j} g^{ij} + [\frac{\partial g^{ij}}{\partial u^i} + \Gamma^k_{ik} g^{ij}] \frac{\partial}{\partial u^j}. \end{aligned}$$

For the problem of 2-D discontinuity localization we adapt the curved coordinate system to the itensity function f in such a way that the first coordinate unit vector $\vec{e}_{u_1} = \vec{e}_{u_n}$ is along the gradient direction of f, while the second coordinate unit vector $\vec{e}_{u_2} = \vec{e}_{u_{n\perp}}$ is locally perpendicular to the first one.

From these definitions we directly find for the metric tensor $g_{ij} = \vec{e}_{u_i} \cdot \vec{e}_{u_j} = \delta_{ij}$. To find the result of the Laplacian operator applied to the intensity function f in these coordinates, we have to insert the metric tensor into the Laplacian, yielding

$$\Delta f = \frac{\partial^2 f}{\partial u_n^2} + \frac{\partial^2 f}{\partial u_{n\perp}^2} + \Gamma^1_{11} \frac{\partial f}{\partial u_n} + \Gamma^2_{12} \frac{\partial f}{\partial u_n} + \Gamma^1_{21} \frac{\partial f}{\partial u_{n\perp}} + \Gamma^2_{22} \frac{\partial f}{\partial u_{n\perp}}.$$

Because we choose $\vec{e}_{u_n}$ along the gradient of f we immediately find $\frac{\partial f}{\partial u_n} = |\nabla f|$, while $\frac{\partial^k f}{\partial u^k_{n\perp}} = 0$ because we choose $\vec{e}_{u_{n\perp}}$ orthogonal to the gradient of f along curves of constant values of f.

Inserting this into Δf and calculating the Chistoffelsymbols by inserting g_{ij} thus yields

$$\begin{aligned}\Delta f &= \frac{\partial^2 f}{\partial u_n^2} + [\vec{e}_{u_{n\perp}} \cdot \frac{\partial \vec{e}_{u_n}}{\partial u_{n\perp}}] \cdot |\nabla f| \\ &= \frac{\partial^2 f}{\partial u_n^2} + \kappa_{isophote} \cdot |\nabla f|,\end{aligned}$$

which represents the shift of the zero crossing location of the Laplacian according to the curvature of the isophote and the local intensity gradient.

There is a second point of view concerning the differential geometry of intesity surfaces, which follows from the noncurved coordinate system defined by the direction of the gradient of f and the orthogonal direction. Let us call these coordinate axes as x_n and $x_{n\perp}$ respectively.

For the surface normal curvature in the gradient direction x_n we find

$$(\kappa_n)_{\theta_\nabla} = \frac{1}{\sqrt{1+(\nabla f)^2}^3} \cdot \frac{\partial^2 f}{\partial x_n^2},$$

from which it has been concluded [45] that zero crossings in κ_n and $\frac{\partial^2 f}{\partial x_n^2}$ must coincide. In addition to this finding we have derived more extensive results. Looking at the normal curvature in the direction orthogonal the gradient direction we find

$$(\kappa_n)_{\theta_\nabla + \frac{\pi}{2}} = \frac{1}{\sqrt{1+(\nabla f)^2}} \cdot \frac{\partial^2 f}{\partial x_{n\perp}^2}.$$

Since for our uncurved coordinate system – $x_n, x_{n\perp}$ – the Laplacian operator is given by $\Delta f = \frac{\partial^2 f}{\partial x_n^2} + \frac{\partial^2 f}{\partial x_{n\perp}^2}$ we can conclude that zero crossings of the Laplacian that coincide with zero crossings of $\frac{\partial^2 f}{\partial x_n^2}$ are always located on intensity surface patches with local zero Gaussian curvature $\kappa = 0$, i.e. locally flat points generated by the boundary of two parabolic patches with opposite sign of mean curvature.

From the two equations for the curvatures given above we can write

$$\Delta f = \sqrt{1+(\nabla f)^2} \cdot [(1+(\nabla f)^2) \cdot (\kappa_n)_{\theta_\nabla} + (\kappa_n)_{\theta_\nabla + \frac{\pi}{2}}]$$

Introducing the principle curvatures κ_1 and κ_2 in accordance to differential geometry as well as the angle ϵ between the direction of normal curvature $(\kappa_n)_{\theta_\nabla}$ and the principal curvature, we find from Euler's formula at points of $\Delta f = 0$ with nonvanishing $\frac{\partial^2 f}{\partial x_{n\perp}^2}$

$$[(\nabla f)^2 + \frac{2+(\nabla f)^2}{\cos 2\epsilon}] \cdot \kappa_1 = [(\nabla f)^2 + \frac{2-(\nabla f)^2}{\cos 2\epsilon}] \cdot \kappa_2.$$

Thus Δf zero crossings *not* coinciding with a zero crossing of the curvature along gradient direction are always located in hyperbolic intensity surface patches, i.e. Gaussian curvature $\kappa < 0$.

Appendix C: Derivation of Equations for Zeroth Order 2-D Model

Content of Appendix C is the derivation of the formulas for the discontinuity localization schemes in two dimensions. Prior to the derivations for the different cases let us summarize the derivatives of the zeroth order 2-D intensity function in polar coordinates

$$\chi(r,\phi) = \mathcal{H}(R-r), \tag{8}$$

where $\mathcal{H}$ denotes the Heaviside function defined by

$$\mathcal{H}(x) = \begin{cases} 1 & \text{if } x \geq 0 \\ 0 & \text{otherwise.} \end{cases}$$

with respect to Polar and Cartesian coordinates as we will need them later:

$$\frac{\partial \chi(r,\phi)}{\partial x} = -\cos\phi \cdot \delta(R-r) \tag{9}$$

$$\frac{\partial \chi(r,\phi)}{\partial y} = -\sin\phi \cdot \delta(R-r) \tag{10}$$

$$\frac{\partial^2 \chi(r,\phi)}{\partial x^2} = \cos^2\phi \cdot \delta'(R-r) - \frac{\sin^2\phi}{r} \cdot \delta(R-r) \tag{11}$$

$$\frac{\partial^2 \chi(r,\phi)}{\partial y^2} = \sin^2\phi \cdot \delta'(R-r) - \frac{\cos^2\phi}{r} \cdot \delta(R-r) \tag{12}$$

$$\Delta\chi(r,\phi) = \frac{1}{r}\delta(R-r) + \delta'(R-r) \tag{13}$$

Here δ denotes the common Delta-distribution and δ' denotes the first order derivative of δ in the usual sense of distributions.

In addition we define the complex n-th order Bessel function [2] as

$$J_n(z) = \frac{-i^n}{\pi} \int_0^\pi \cos(n\theta) e^{iz\cos\theta} d\theta,$$

and the modified n-th order Bessel function

$$I_n(z) = e^{-\frac{i\pi n}{2}} J_n(ze^{\frac{i\pi}{2}})$$

Appendix C.1: Laplacian of Gaussian

This Appendix contains the derivation of the formula for the the Laplacian of Gaussian applied to the zeroth order 2-D model.

The convolution of the intensity function (eqn. (8)) with the Laplacian of the Gaussian

$$G(r,\phi) = N_\sigma \exp(-\frac{r^2}{2\sigma^2})$$

is

$$(\chi \otimes \Delta G)(r,\phi) = (\Delta\chi \otimes G)(r,\phi).$$

With the Laplacian operator in polar coordinates applied to the zeroth order 2-D function as given in (eqn. (13)) the convolution of the Laplacian of Gausian and $\mathcal{H}$ in polar coordinates yields

$$\begin{aligned}(\Delta\chi \otimes G)(r,\phi) &= N_\sigma \cdot \int_0^\infty \int_0^{2\pi} r' dr' d\phi' [(\frac{1}{r'}\delta(R-r') + \delta'(R-r')) \cdot \\ &\quad \cdot \exp(-\frac{r'^2 + r^2 - 2rr'\cos(\phi'-\phi)}{2\sigma^2})],\end{aligned}$$

where we have used the identity

$$\cos(\phi' - \phi) = \cos\phi\cos\phi' + \sin\phi\sin\phi'.$$

With the definition of the complex zeroth order Bessel function

$$J_0(z) = \frac{1}{\pi}\int_0^\pi exp(-iz\cos\beta)d\beta$$

the integration over ϕ' can be done and one yields

$$\begin{aligned}(\Delta\chi \otimes G)(r,\phi) &= 2\pi N_\sigma (\int_0^\infty dr'\delta(R-r')\exp(-\frac{r'^2+r^2}{2\sigma^2})J_0(i\frac{rr'}{\sigma^2}) \\ &\quad + \int_0^\infty dr' r'\delta'(R-r')\exp(-\frac{r'^2+r^2}{2\sigma^2})J_0(i\frac{rr'}{\sigma^2})) \\ &= 2\pi N_\sigma (\exp(-\frac{R^2+r^2}{2\sigma^2})\cdot J_0(i\frac{Rr}{\sigma^2}) \\ &\quad + \int_0^\infty dr' r'\delta'(R-r')\exp(-\frac{r'^2+r^2}{2\sigma^2})J_0(i\frac{rr'}{\sigma^2}))\end{aligned}$$

where we have finally evaluated the δ distribution in the first integral.

Because of

$$\begin{aligned}\int_0^\infty \delta'(x)f(x)dx &= -f'(0) \\ \frac{\partial J_0(x)}{\partial x} &= -J_1(x),\end{aligned}$$

where J_1 denotes the first order Bessel function, we can evaluate the second integral in accordance to the definition of the δ' distribution

$$
\begin{aligned}
(\Delta\chi \otimes G)(r,\phi) &= 2\pi N_\sigma \exp(-\frac{R^2+r^2}{2\sigma^2}) \cdot J_0(i\frac{Rr}{\sigma^2}) \\
&\quad + 2\pi N_\sigma \frac{\partial}{\partial r'}(r' \cdot \exp(-\frac{r'^2+r^2}{2\sigma^2}) \cdot J_0(i\frac{rr'}{\sigma^2}))_{r'=R} \\
&= 2\pi N_\sigma \exp(-\frac{R^2+r^2}{2\sigma^2}) \cdot J_0(i\frac{Rr}{\sigma^2}) \\
&\quad - 2\pi N_\sigma \exp(-\frac{R^2+r^2}{2\sigma^2}) \cdot J_0(i\frac{Rr}{\sigma^2}) \\
&\quad + 2\pi N_\sigma \frac{R^2}{\sigma^2} \cdot \exp(-\frac{R^2+r^2}{2\sigma^2}) \cdot J_0(i\frac{Rr}{\sigma^2}) \\
&\quad + 2\pi N_\sigma i\frac{Rr}{\sigma^2} \cdot \exp(-\frac{R^2+r^2}{2\sigma^2}) \cdot J_1(i\frac{Rr}{\sigma^2})
\end{aligned}
$$

Thus we can finally express the result of the convolution as

$$
(\Delta\chi \otimes G)(r,\phi) = 2\pi N_\sigma \frac{R^2}{\sigma^2} \cdot \exp(-\frac{R^2+r^2}{2\sigma^2}) \cdot (J_0(i\frac{R^2}{\sigma^2}\frac{r}{R}) + i\frac{r}{R}J_1(i\frac{R^2}{\sigma^2}\frac{r}{R}))
$$

Hence for the zero crossings we get

$$
(\Delta\chi \otimes G)(r,\phi) = 0 \iff J_0(i\frac{R^2}{\sigma^2}\frac{r}{R}) + i\frac{r}{R}J_1(i\frac{R^2}{\sigma^2}\frac{r}{R}) = 0.
$$

With the only free parameter as $\alpha = R/\sigma$ and introducing the normalized radius $\hat{r} = r/R$ this finally yields the equation

$$
J_0(i\alpha^2\hat{r}) + i\hat{r}J_1(i\alpha^2\hat{r}) = 0,
$$

which simplifies in terms of the modified Bessel functions as defined above to

$$
I_0(\alpha^2\hat{r}) - \hat{r}I_1(\alpha^2\hat{r}) = 0.
$$

Appendix C.2: First Order Directional Derivative

This appendix contains the derivation of the formula for the points of maxima within the first order directional derivative of the Gaussian filtered, zeroth order 2-D intensity function. Because of the overall circular symmetry of the problem, we can restrict ourself to one specific direction for the differentiation without any loss of generality. Therefore we take the partial derivative with respect to the x-direction.

A necessary and sufficient condition for the maximum we are looking for is the vanishing of the second order derivative with respect to x, because we only search for the maximum along the x-direction. Thus with the Gaussian as defined above, we have to calculate

$$
(\frac{\partial^2\chi}{\partial x^2} \otimes G)(r,\phi) = 0
$$

Let us first calculate the convolution for the second order derivative with respect to x.

Inserting the result of the derivatives (eqn. (9-12)) into the convolution with the Gaussian in the very same way as for the Laplacian of Gaussian yields

$$(\chi_{xx} \otimes G)(r,\phi) = N_\sigma \int_0^\infty \int_0^{2\pi} r' dr' d\phi' [(\mathcal{F}_1(r',\phi') - \mathcal{F}_2(r',\phi')) \cdot \tag{14}$$

$$\cdot \exp(-\frac{r'^2 + r^2 - 2rr'\cos(\phi' - \phi)}{2\sigma^2})], \tag{15}$$

where we have defined

$$\begin{aligned} \chi_{xx}(r',\phi') &= \frac{\partial^2 \chi}{\partial x^2}(r',\phi') \\ \mathcal{F}_1(r',\phi') &= \cos^2\phi' \cdot \delta'(R - r') \\ \mathcal{F}_2(r',\phi') &= \frac{\sin^2\phi'}{r'} \cdot \delta(R - r') \end{aligned}$$

The two integrals for $\mathcal{F}_1$ and $\mathcal{F}_2$ are calculated sequentially within the following subsections.

First Integral

The integral over $\mathcal{F}_1$ is abbreviated as $F1(r,\phi)$ and can be written

$$F1(r,\phi) = N_\sigma \exp(-\frac{r^2}{2\sigma^2}) \int_0^\infty dr' r' \delta'(R - r') \exp(-\frac{r'^2}{2\sigma^2}) \mathcal{F}_{1\phi},$$

where we have defined

$$\mathcal{F}_{1\phi} = \int_0^{2\pi} d\phi' \cos^2\phi' \exp[\frac{rr'}{\sigma^2}\cos(\phi' - \phi)].$$

Using some trigonometric identities one can verify

$$\cos^2\phi' = \frac{1}{2}(1 + \cos 2\phi \cos 2(\phi' - \phi) - \sin 2\phi \sin 2(\phi' - \phi)).$$

Inserting this identity for $\cos^2\phi'$ into $\mathcal{F}_{1\phi}$ leaves us with three terms for integration over ϕ' :

$$\begin{aligned} \mathcal{F}_{1\phi,1} &= \frac{1}{2}\int_0^{2\pi} d\phi' \exp(\frac{rr'}{\sigma^2}\cos(\phi' - \phi)) \\ &= \pi J_0(-i\frac{rr'}{\sigma^2}), \end{aligned}$$

$$\begin{aligned}
\mathcal{F}_{1\phi,2} &= \frac{1}{2}\int_0^{2\pi} d\phi' \exp(\frac{rr'}{\sigma^2}\cos(\phi'-\phi))\cdot\cos 2\phi\cos 2(\phi'-\phi) \\
&= \cos 2\phi\int_0^{2\pi} d\phi' \exp(-i\frac{rr'}{\sigma^2}\cos\phi')\cdot\cos 2\phi' \\
&= -2\pi\cos 2\phi J_2(-i\frac{rr'}{\sigma^2}) \quad , and \\
\mathcal{F}_{1\phi,3} &= \frac{1}{2}\int_0^{2\pi} d\phi' \exp(\frac{rr'}{\sigma^2}\cos(\phi'-\phi))\cdot\sin 2\phi\sin 2(\phi'-\phi) \\
&= 0.
\end{aligned}$$

The vanishing of $\mathcal{F}_{1\phi,3}$ can be easily seen by symmetry arguments.

Collecting together the three terms finally yields

$$\mathcal{F}_{1\phi} = \pi\cdot(J_0(-i\frac{rr'}{\sigma^2}) - \cos 2\phi\cdot J_2(-i\frac{rr'}{\sigma^2})).$$

Now we can solve for $F1$ inserting $\mathcal{F}_{1\phi}$ into the integral for $F1$ by evaluation of the δ' distribution, yielding

$$\begin{aligned}
F1(r,\phi) &= \pi N_\sigma \exp(-\frac{r^2}{2\sigma^2})\cdot \\
&\quad \frac{\partial}{\partial r'}[r'\exp(-\frac{r'^2}{2\sigma^2})\cdot(J_0(-i\frac{rr'}{\sigma^2}) - \cos 2\phi J_2(-i\frac{rr'}{\sigma^2}))]_{r'=R}.
\end{aligned}$$

Using the general identities for Bessel functions

$$\begin{aligned}
\frac{\partial}{\partial z}(z^n J_n(z)) &= z^n J_{n-1}(z) \quad and \\
J_{-n}(z) &= (-1)^n J_n(z),
\end{aligned}$$

the derivations of the terms corresponding to the two Bessel functions can be done in a straight forward manor, yielding

$$\frac{\partial}{\partial r'}[r'\exp(-\frac{r'^2}{2\sigma^2})J_0(-i\frac{rr'}{\sigma^2})]_{r'=R} =$$

$$\exp(-\frac{R^2}{2\sigma^2})\cdot[(1-\alpha^2)J_0(-i\alpha^2\hat{r}) + i\alpha^2\hat{r}J_1(-i\alpha^2\hat{r})]$$

and

$$\frac{\partial}{\partial r'}[-r'\exp(-\frac{r'^2}{2\sigma^2})\cos 2\phi J_2(-i\frac{rr'}{\sigma^2})]_{r'=R} =$$

$$exp(-\frac{R^2}{2\sigma^2})\cos 2\phi\cdot[(1+\alpha^2)J_2(-i\alpha^2\hat{r}) + i\alpha^2\hat{r}J_1(-i\alpha^2\hat{r})],$$

where we have defined $\alpha = R/\sigma$ and $\hat{r} = r/R$ again. Collecting together the two terms for the final result of the first integral $F1$, we arrive at

$$\begin{aligned}
F1(r,\phi) &= \pi N_\sigma \exp(-\frac{r^2+R^2}{2\sigma^2})\cdot[(1+\alpha^2)\cos 2\phi J_2(-i\alpha^2\hat{r}) + \\
&\quad +(1-\alpha^2)J_0(-i\alpha^2\hat{r}) + i\alpha^2\hat{r}(1+\cos 2\phi)J_1(-i\alpha^2\hat{r})]
\end{aligned}$$

Second Integral

To calculate the final result of the convolution (eqn. (14)) we have to solve the integral over $\mathcal{F}_2$, which we abbreviate as $F2(r,\phi)$ for simplicity of notations. We find

$$F2(r,\phi) = -N_\sigma \exp(-\frac{r^2}{2\sigma^2}) \int_0^\infty dr' \delta(R-r') \exp(-\frac{r'^2}{2\sigma^2}) \mathcal{F}_{2\phi},$$

where we have defined

$$\mathcal{F}_{2\phi} = \int_0^{2\pi} d\phi' \sin^2\phi' \exp[-\frac{rr'}{\sigma^2}\cos(\phi'-\phi)]$$

analogous to the first integral. Simply enough it holds that

$$\sin^2\phi' = \frac{1}{2}(1 - \cos 2\phi \cos 2(\phi'-\phi) + \sin 2\phi \sin 2(\phi'-\phi)).$$

Inserting this into $\mathcal{F}_{2\phi}$ and comparing the resulting integrals with the coresponding integrals of $\mathcal{F}_{1\phi}$ we immediately see that

$$\mathcal{F}_{2\phi} = \mathcal{F}_{1\phi,1} - \mathcal{F}_{1\phi,2} - \mathcal{F}_{1\phi,3}.$$

From the results for $\mathcal{F}_{1\phi}$ we get

$$\mathcal{F}_{2\phi} = \pi \cdot (J_0(-i\frac{rr'}{\sigma^2}) + \cos 2\phi \cdot J_2(-i\frac{rr'}{\sigma^2})),$$

and we can solve the integral for $F2(r,\phi)$ after inserting $\mathcal{F}_{2\phi}$ into the integral for $F2$ by simply evaluating the δ distribution. With our abbreviations α and $\hat{r}$ from above we get

$$F2(r,\phi) = -\pi N_\sigma \exp(-\frac{r^2+R^2}{2\sigma^2}) \cdot [\cos 2\phi J_2(-i\alpha^2\hat{r}) + J_0(-i\alpha^2\hat{r})]$$

The Zero Crossings

Collecting together $F1$ and $F2$ we finally yield

$$(\chi_{xx} \otimes G)(r,\phi) = F1(r,\phi) + F2(r,\phi) =$$
$$\pi N_\sigma \exp(-\frac{r^2+R^2}{2\sigma^2})\alpha \cdot [\cos 2\phi J_2(i\alpha^2\hat{r}) - J_0(i\alpha^2\hat{r}) - i(1+\cos 2\phi)\hat{r}J_1(i\alpha^2\hat{r})],$$

where we have used another identity for Bessel functions

$$J_n(z) = (-1)^n J_n(-z).$$

Finally we introduce the modified Bessel functions to get the result for the zero crossings of the convolution to be

$$I_0(\alpha\hat{r}) + \cos 2\phi \cdot I_2(\alpha\hat{r}) - (1+\cos 2\phi)\cdot\hat{r}\cdot I_1(\alpha\hat{r}) = 0$$

Appendix D: On Higher Order 2-D Models

Within this final appendix, we discuss a possible extension for the derivation of the equation for zero crossings of the Laplacian of Gaussian to higher order models of 2-D intensity functions.

Let therefore the contour of the object be described by the dependence of the radius R on the polar angle ϕ. Restricting to closed contours $R(0) = R(2\pi)$, we can expand $R(\phi)$ into a Fourier series yielding

$$R(\phi) = R_0 + [\sum_{k=1}^{\infty} a_k \cos k\phi + b_k \sin k\phi],$$

where the a_k and b_k are sometimes called *Fourier Descriptors* within the image analysis literature.

In generalization to Appendix C, we now have

$$\chi(r, \phi) = \mathcal{H}(R(\phi) - r)$$

and we additionally have to take care of the ϕ term within the Laplacian operator in polar coordinates

$$\Delta = \frac{1}{r} \cdot \frac{\partial}{\partial r}(r \cdot \frac{\partial}{\partial r}) + \frac{1}{r^2} \cdot \frac{\partial^2}{\partial \phi^2}$$

which we could neglect in Appendix C.

The result of the $r-$term of the Laplace operator can be taken from Appendix C.1 by simply replacing R by $R(\phi)$. For the evaluation of the $\phi-$term, we abbreviate

$$F_k(\phi) = a_k \cos k\phi + b_k \sin k\phi,$$

such that we have

$$\chi(r, \phi) = \mathcal{H}(R_0 + [\sum_{k=1}^{\infty} F_k(\phi)] - r).$$

The second partial derivative with respect to ϕ can be done straight forward, using the definitions of the δ distribution and its derivative.
We get

$$\begin{aligned} \frac{\partial^2 \chi(r, \phi)}{\partial \phi^2} &= [\sum_{k=1}^{\infty} F_k(\phi)]^2 \cdot \frac{1}{r^2} \cdot \delta'(R_0 + [\sum_{k=1}^{\infty} F_k(\phi)] - r) \\ &\quad -[\sum_{k=1}^{\infty} k^2 F_k(\phi)] \cdot \frac{1}{r^2} \cdot \delta(R_0 + [\sum_{k=1}^{\infty} F_k(\phi)] - r). \end{aligned}$$

Collecting together the terms for the derivatives with respect to r and ϕ respectively finally yields

$$\Delta\chi(r,\phi) = (\frac{1}{r} - [\sum_{k=1}^{\infty} k^2 F_k(\phi)] \cdot \frac{1}{r^2}) \cdot \delta(R_0 + [\sum_{k=1}^{\infty} F_k(\phi)] - r)$$
$$+(1 + [\sum_{k=1}^{\infty} F_k(\phi)]^2 \cdot \frac{1}{r^2}) \cdot \delta'(R_0 + [\sum_{k=1}^{\infty} F_k(\phi)] - r)$$

This two terms now have to be convolved with the Gaussian.

Let us outline the general way of solving these integrals for the first term of $\Delta\chi$.

First the integration over r' is done by evaluating the δ distribution, so that we find the integral over ϕ' to be solved:

$$(\Delta\chi \otimes G)_{1st}(r,\phi) = \int_0^{2\pi} d\phi'(1 + \frac{[\sum_{k=1}^{\infty} k^2 F_k(\phi')]}{(R_0 + [\sum_{k=1}^{\infty} F_k(\phi')])}) \cdot$$
$$\exp[-\frac{1}{2\sigma^2}[r^2 + (R_0 + [\sum_{k=1}^{\infty} F_k(\phi')])^2 - 2r(R_0 + [\sum_{k=1}^{\infty} F_k(\phi')])\cos(\phi' - \phi)])]$$

Assume that the contour can be described by a finite number N of Fourier descriptors, so that the infinite series become finite sums. Finding the ratio of sums containing $\cos k\phi'$ and $\sin k\phi'$ within the intergal leads directly to the substitution $z = \exp(i\phi')$. This will

- transfer the real integral from 0 to 2π to an integral within the complex plane over the unit circle $|z| = 1$ and $d\phi = \frac{-i}{z} dz$.
- make the finite sums of $\cos k\phi'$ and $\sin k\phi'$ terms simply a polynomial in z, because $\cos(k\phi') = \frac{1}{2}(z^k + z^{-k})$ and $\sin(k\phi') = \frac{1}{2i}(z^k - z^{-k})$.

Thus we will find after the substitution

$$(\Delta\chi \otimes G)_{1st}(r,\phi) = \oint_{|z|=1} dz \frac{P_d(z)}{P_n(z)} \cdot \exp[-P_e(z,r,\phi)],$$

where $P_d(z), P_n(z)$ and $P_e(z)$ are polynomials in z whose coefficients depend simply on the Fourier descriptors of the contour.

The solution of this type of integral is straight forward using the *residue theorem* from complex analysis:

Let G be a domain within the complex plane C, and $S \subset G$ a discrete set of points such that the function f from $G \backslash S$ into C is *holomorphic*. The points within S are thus isolated singularities of f. Let Γ be a closed path within C and let $\Gamma \cap S = \emptyset$, than

$$\oint_\Gamma dz f(z) = 2\pi i \cdot [\sum_{s \in S} w_\Gamma(s) res_s(f)],$$

where $res_s(f)$ is the first negative coefficient of the Laurent series of f, and $w_\Gamma(s)$ is the winding number of Γ with respect to s.

Is $f(z) = \frac{g(z)}{z-s}$, as it is for our cases, $res_s(f) = g(s)$.

To apply the theorem to our integral we have to

- identify the set of singularity points of our integrand. These singularities are obviously given by the zeros of the nominater polynomial $P_n(z)$. We thus solve for all zeros of P_n, which gives us the set S.
- calculate the winding numbers of our path with respect to each $s \in S$. Because we integrate over the boundary of the unit circle $|z| = 1$, the winding number for each s is simply 1, when s lies within the unit circle $|s| < 1$, and the winding number is 0 else. We thus have to determine the subset $S' \subset S$ of zeros of P_n within the unit circle.
- for each $s \in s'$ we finally calculate the residuum simply by factoring out $(z - s)$ from $P_n(z)$, and inserting s into the remaining function within the integral using the rule for residua given above.

References

[1] Abdou, I.E.; Pratt, W.K.: Quantitative design and evaluation of enhancement/thresholding edge detectors. Proceedings of the IEEE 67:5 (1979), 753-763.

[2] Abramowitz, M.; Stegun, I.A. (Eds.): Handbook of Mathematical Functions (9th printing). Dover Publ., New York (1972).

[3] Babaud, J.; Witkin, A.P.; Baudin, M.; Duda, R.O.: Uniqueness of the Gaussian Kernel for Scale-Space Filtering. IEEE Trans. on Pattern Analysis and Machine Intelligence 8:1 (1986), 26-33.

[4] Back, S.; Neumann, H.; Stiehl, H.S.: On Scale-Space Edge Detection in Computed Tomograms. in: Burckhardt, H.; Hoehne, K.-H.; Neumann, B. (Eds.), Mustererkennung 1989. Informatik-Fachberichte 219, Springer-Verlag (1989), 216-223

[5] Bergholm, F.: Edge Focusing. Royal Institute of Technology (Stockholm, Sweden), Dept. of Numerical Analysis and Computing Science, Report TRITA-NA-8518 (1985).

[6] Bergholm, F.: On the Content of Information in Edges and Optical Flow. Royal Institute of Technology (Stockholm, Sweden), Dept. of Numerical Analysis and Computing Science, Report TRITA-NA-P8904 (Dissertation) (1989).

[7] Berzins, V.: Accuracy of Laplacian Edge Detectors. Computer Vision, Graphics, and Image Processing 27:2 (1984), 195-210.

[8] Binford, T.O.: Inferring Surfaces from Images. Artificial Intelligence 17:1-3 (1981), 205-244.

[9] Bracewell, R.N.: The Fourier Transform and its Applications. McGraw-Hill, New York (1976).

[10] Canny, J.F.: A Variational Approach to Edge Detection. Proc. of the National Conf. on Artificial Intelligence, AAAI-83, Wash. DC, USA (1983), 54-58.

[11] Canny, J.F.: Finding Edges and Lines in Images. MIT, AI Laboratory, TR No.720 (1983).

[12] Canny, J.F.: A Computational Approach to Edge Detection. IEEE Trans. on Pattern Analysis and Machine Intelligence 8:6 (1986), 679-698.

[13] Chen, J.S.; Medioni, G.: Detection, Localization, and Estimation of Edges. IEEE Trans. on Pattern Analysis and Machine Intelligence 11:2 (1989), 191-198.

[14] Clark, J.J.: Singularities of Contrast Functions in Scale Space. Proc. 1st Int. Conf. on Computer Vision ICCV, London, GB, June 8-11, 1987, 491-495.

[15] Clark, J.J.: Authenticating Edges Produced by Zero-Crossing Algorithms. IEEE Trans. on Pattern Analysis and Machine Intelligence 11:1 (1989), 43-57.

[16] doCarmo, M.P.: Differential Geometry of Curves and Surfaces. Prentice-Hall (1976).

[17] Evans, J.M.; Kirsch, R.; Nagel, R.N. (Eds.): Standards for Image Pattern Recognition (Proc. of a Workshop, Gathersburg, USA (1976)). U.S. Department of Commerce, National Bureau of Standards, Publication 500-8 (1977).

[18] Geiger, D.; Poggio, T.: An Optimal Scale for Edge Detection. Proceedings of the IJCAI'87, Milano, 745-748.

[19] Gennert, M.A.: Detecting Half-Edges and Vertices in Images. Proc. Int. Conf. on Computer Vision and Pattern Recognition, Miami Beach, USA, June 22-26, 1986, 552-557.

[20] Haralick, R.M.: Digital Step Edges from Zero-Crossings of Second Directional Derivative. IEEE Trans. on Pattern Analysis and Machine Intelligence 6:1 (1984), 55-68.

[21] Haralick, R.M.: Computer Vision Theory: The Lack Thereof. Proc. 3rd Workshop on Computer Vision: Representation and Control, Bellaire, Mich., USA (1985) 113-121.

[22] Haralick, R.M.: Machine Vision Mensuration (Preface). Computer Vision, Graphics, and Image Processing 40 (1987), 271-272.

[23] Horn, B.K.P.: Understanding Image Intensities. Artificial Intelligence 8:2 (1977), 201-231.

[24] Huertas, A.; Medioni, G.: Detection of Intensity Changes with Subpixel Accurracy Using Laplacian of Gaussian Masks. IEEE Trans. on Pattern Analysis and Machine Intelligence 8:5 (1986), 651-664.

[25] Hummel, R.; Lowe, D.: Computational Considerations in Convolution and Feature-Extraction in Images. in: Simon, J.C. (Ed.): From Pixels to Features. North-Holland, Amsterdam (1989), 91-102.

[26] Kitchen, L.J.; Malin, J.A.: The Effect of Spatial Discretization on the Magnitude and Direction Response of Simple Differential Edge Operators on a Step Edge. Computer Vision, Graphics and Image Processing 47 (1989), 243-258.

[27] Korn, A.: Towards a Symbolic Representation of Intensity Changes in Images. IEEE Trans. on Pattern Analysis and Machine Intelligence 10:5 (1988), 610-625.

[28] Levine, M.D.: Vision in Man and Machine. McGraw Hill, New York (1985).

[29] Lutscher, W.H.H.; Beddoes, M.P.: Optimal Edge Detector Design I, II. IEEE Trans. on Pattern Analysis and Machine Intelligence 8:2 (1986), 164-177, 178-187.

[30] Marr, D.; Hildreth, E.C.: Theory of Edge Detection. Proc. Royal Soc. of London 207 (B) (1980) 187-217.

[31] Marr, D.: Vision - A Computational Investigation into the Human Representation of Processing of Visual Information. W.H.Freeman, San Francisco (1982).

[32] Nagel, H.-H.: Displacement Vectors Derived from Second-Order Intensity Variations in Image Sequences. Computer Vision, Graphics, and Image Processing 21:1 (1983), 85-117.

[33] Nagel, H.-H.: Principles of (Low-Level) Computer Vision. in: Haton, J.P. (Ed.): Fundamentals in Computer Understanding: Speech, Vision, and Natural Language (1985). Cambridge University Press.

[34] Nalwa, V.S; Binford, T.O.: On Detecting Edges. IEEE Trans. on Pattern Analysis and Machine Intelligence 8:6 (1986), 699-714.

[35] Neumann, H.; Stiehl, H.S.: Toward a Testbed for Evaluation of Early Vision Processes, in: Yaroslavskii, L.P.; Rosenfeld, A.; Wilhelmi, W. (Eds.) Computer Analysis of Images and Patterns. Mathematical Research Vol 40, Akademi-Verlag Berlin (1987), 202-208.

[36] Lei, G.: Level Crossing Curvature and the Laplacian. Image and Vision Computing 6:3 (1988), 185-188.

[37] Levine, M.D.: Vision in Man and Machine. McGraw-Hill, New York (1985).

[38] Lu, Y.; Jain, R.C.: Behavior of Edges in Scale Space. IEEE Trans. on Pattern Analysis and Machine Intelligence 11:4 (1989), 337-356.

[39] Lüke, H.D.: Signalübertragung. Springer, Berlin (3rd Print, 1985).

[40] Oppenheim, A.V.; Willsky, A.S.: Signals and Systems. Prentice-Hall, London (1983).

[41] Piech, M.A.: Comments on Fingerprints of Two-Dimensional Edge Models. Computer Vision, Graphics, and Image Processing 42 (1988), 381-386.

[42] Price, K.: I've Seen Your Demo: So What? Proc. 3rd Workshop on Computer Vision: Representation and Control, Bellaire, Mich., USA, Oct. 13-14 (1985), 122-124. (see also: Price, K.: Anything You Can Do, I Can Do Better (No You Can't ...), Computer Vision, Graphics, and Image Processing 36:2 (1987), 387-391.)

[43] Shah, M.; Sood, A.; Jain, R.: Pulse and Staircase Models for Detecting Edges at Multiple Resolution. Proc. 3rd Workshop on Computer Vision: Representation and Control, Bellaire, Mich., USA, Oct. 13-14 (1985), 84-95.

[44] Spacek, L.A.: Edge Detection and Motion Detection. Image and Vision Computing 4:1 (1986), 43-56.

[45] Torre, V.; Poggio, T.: On Edge Detection. IEEE Trans. on Pattern Analysis and Machine Intelligence 8:2 (1986), 147-163.

[46] van Warmerdam, W.L.G; Algazi, V.R.: Decsribing 1-D Intensity Transitions with Gaussian Derivatives at the Resolutions Matching the Transition Widths. IEEE Trans. on Pattern Analysis and Machine Intelligence 11:9 (1989), 973-977.

[47] Yuille, A.; Poggio, T.: Scaling Theorems for Zero-Crossings. MIT, AI Laboratory, Memo 722 (1983).

[48] Yuille, A.; Poggio, T.: Fingerprint Theorems for Zero-Crossings. MIT, AI Laboratory, Memo 730 (1983).